AIAA 2002-3239
Geometric, Kinematic and Radiometric Aspects of Image-Based Measurements

Tianshu Liu

NASA Langley Research Center
Hampton, VA 23681-2199

22nd AIAA Aerodynamic Measurement Technology and Ground Testing Conference
24-26 June 2002/St. Louis, Missouri

AIAA 2002-3239

Geometric, Kinematic and Radiometric Aspects of Image-Based Measurements

Tianshu Liu†
NASA Langley Research Center, Hampton, VA 23681-0001

Abstract

This paper discusses theoretical foundations of quantitative image-based measurements for extracting and reconstructing geometric, kinematic and dynamic properties of observed objects. New results are obtained by using a combination of methods in perspective geometry, differential geometry, radiometry, kinematics and dynamics. Specific topics include perspective projection transformation, perspective developable conical surface, perspective projection under surface constraint, perspective invariants, the point correspondence problem, motion fields of curves and surfaces, and motion equations of image intensity. The methods given in this paper are useful for determining morphology and motion fields of deformable bodies such as elastic bodies, viscoelastic mediums and fluids.

Table of Contents

1. Introduction

Image-based measurement techniques play an increasingly important role in virtually all natural sciences and engineering disciplines since they can provide tremendous information and knowledge about observed objects in a global, non-contact way with high temporal and spatial resolution. Specialists in photogrammetry, computer vision, and other scientific and engineering disciplines have developed various methods that are best suitable to particular applications in their fields. In particular, both photogrammetrists and computer vision scientists have studied image-based techniques for many years to obtain metric and geometric information. The approaches developed by photogrammetrists are more mature and quantitative, which are recently extended to non-topographic applications [1]. By contrast, in order to deal with more complicated vision problems related to artificial intelligence, computer scientists tend to adopt more versatile mathematical approaches in perspective geometry, differential geometry and image algebra [2-5]. However, the approaches used by computer vision scientists are of qualitative nature in many cases and generally less accurate than those used in photogrammetry in metric measurements. Because the objectives of different disciplines are very different, there is a lack of sufficient interaction among specialists in various technical communities. Perhaps due to different notations, jargons and methodologies in these communities, it is difficult to transcend the different technical domains and see a unified scope of various image techniques.

From a methodological standpoint, the approaches in photogrammetry and computer vision should be integrated into a universal theoretical framework. Furthermore, unlike computer vision scientists who mainly study rigid bodies, aerospace engineers and scientists often deal with complex morphology and motion fields of deformable bodies such as elastic bodies, viscoelastic mediums and fluids. It is highly desirable to formulate universal theoretical foundations for quantitative image-based measurements of morphology and motion fields of deformable bodies. In this paper, we will focus on the geometric, kinematic and radiometric aspects of image-based measurements. First, we will provide a unified treatment of the perspective projection transformation from the 3D object space to the 2D image plane and illustrate geometric connections among different formulations of the perspective projection transformation. Then, we will discusses some specific problems for recovering geometry and motion, such as projective developable conical surface, projection under surface constraint, reconstruction of motion field on a surface and motion field of a 3D curve, the correspondence problem, and projective invariants. This is an area for combined application of approaches in perspective geometry, differential geometry, kinematics and dynamics. In the

† Research Scientist, Model Systems Branch, MS 238, Member AIAA

radiometric aspect, we will discuss the fundamental relationship between the image intensity and radiance from an object. Based on this relation and imposed physical constraints, the motion equations of image intensity will be derived for typical physical processes such as moving Lamertian surface, emitting passive scalar transport, and transmitting passive scalar transport. These equations provide a rational way for reconstructing the geometric and kinematic properties of deformable bodies like fluids. In general, the geometric, kinematic and radiometric approaches are closely coupled.

2. Perspective Projection Transformation from 3D Space to 2D Image

Image-based measurement techniques extract data from 2D images and then map them into the 3D object space. There is a perspective relationship between the 3D coordinates in the object space and the corresponding 2D coordinates in the image plane [1, 6-8]. Here, we discuss several formulations of the perspective projection transformation. Although these formulations are equivalent, one may be more convenient to use than others for a specific problem. The fundamental geometric problem in image-based measurements is to determine the object space coordinates $\boldsymbol{X} = (X^1, X^2, X^3)^T$ given the corresponding image (retinal) coordinates $\boldsymbol{x} = (x^1, x^2)^T$. Figure 1 illustrates the camera imaging process. The lens of the camera is modeled by a single point known as the perspective center (or the optical center), the location of which in the object space is $\boldsymbol{X_c} = (X_c^1, X_c^2, X_c^3)^T$. Likewise, the orientation of the camera is characterized by three Euler orientation angles. The orientation angles and location of the perspective center are referred to as the exterior orientation parameters. The object space point, perspective center and image point lie along a straight line for a "perfect" camera. This relationship is described by the collinearity equations, the fundamental equations of photogrammetry. On the other hand, the relationship between the perspective center and the image coordinate system is defined by the camera interior orientation parameters, namely, the camera principal distance *c* and the photogrammetric principal-point location $\boldsymbol{x_p} = (x_p^1, y_p^2)^T$. The principal distance *c*, which equals the camera focal length for a camera focused at infinity, is the perpendicular distance from the perspective center to the image plane, whereas the photogrammetric principal-point is where a perpendicular line from the perspective center intersects the image plane. Due to the lens distortion, however, perturbations to the imaging process lead to departures from collinearity that can be represented by the shifts δx^1 and δx^2 of the image point from its "ideal" position on the image plane. The shifts δx^1 and δx^2 are modeled and characterized by a number of the lens distortion parameters.

The image and object space coordinates of the points are related by the collinearity condition in which the image vector is aligned with the vector from the perspective center to the object space point

$$\begin{pmatrix} x^1 - x_p^1 + \delta x^1 \\ x^2 - x_p^2 + \delta x^2 \\ -c \end{pmatrix} = \lambda \boldsymbol{M} \begin{pmatrix} X^1 - X_c^1 \\ X^2 - X_c^2 \\ X^3 - X_c^3 \end{pmatrix}, \qquad (2.1)$$

where $\boldsymbol{M} = [m_{ij}]$ is the rotation matrix, λ is a scaling factor. Algebraic manipulation of Eq. (2.1) yields the well-known collinearity equations (with the distortion terms δx^1 and δx^2) relating the point in the 3D object space to the corresponding point on the image plane,

$$\begin{aligned} x^1 - x_p^1 + \delta x^1 &= -c \frac{\boldsymbol{m_1}^T (\boldsymbol{X} - \boldsymbol{X_c})}{\boldsymbol{m_3}^T (\boldsymbol{X} - \boldsymbol{X_c})} = -c \frac{\overline{X}^1}{\overline{X}^3} \\ x^2 - x_p^2 + \delta x^2 &= -c \frac{\boldsymbol{m_2}^T (\boldsymbol{X} - \boldsymbol{X_c})}{\boldsymbol{m_3}^T (\boldsymbol{X} - \boldsymbol{X_c})} = -c \frac{\overline{X}^2}{\overline{X}^3} \end{aligned}, \qquad (2.2)$$

where the vectors $\boldsymbol{m_1} = (m_{11}, m_{12}, m_{13})^T$ and $\boldsymbol{m_2} = (m_{21}, m_{22}, m_{23})^T$ are the directional cosine vectors along the x^1-axis, x^2-axis in the image plane, respectively. The vector $\boldsymbol{m_3} = (m_{31}, m_{32}, m_{33})^T$ is normal to the image plane, directing from the principal point to the optical center on the optical axis. As shown in Fig. 1, the unit orthogonal vectors $\boldsymbol{m_1}$, $\boldsymbol{m_2}$, and $\boldsymbol{m_3}$ constitute an object space coordinate frame at the optical center $\boldsymbol{X_c}$ and $\overline{\boldsymbol{X}} = (\overline{X}^1, \overline{X}^2, \overline{X}^3)^T$ are the projections of the object space position vector $\boldsymbol{X} - \boldsymbol{X_c}$ in this frame. The elements of the rotation matrix m_{ij} *(i, j = 1, 2, 3)* are functions of the Euler orientation angles (ω, ϕ, κ),

$$\begin{aligned} &m_{11} = \cos\phi \cos\kappa, \quad m_{12} = \sin\omega \sin\phi \cos\kappa + \cos\omega \sin\kappa, \\ &m_{13} = -\cos\omega \sin\phi \cos\kappa + \sin\omega \sin\kappa, \quad m_{21} = -\cos\phi \sin\kappa, \\ &m_{22} = -\sin\omega \sin\phi \sin\kappa + \cos\omega \cos\kappa, \\ &m_{23} = \cos\omega \sin\phi \sin\kappa + \sin\omega \cos\kappa, \\ &m_{31} = \sin\phi, \quad m_{32} = -\sin\omega \cos\phi, \quad m_{33} = \cos\omega \cos\phi. \end{aligned} \qquad (2.3)$$

The orientation angles (ω, ϕ, κ) are essentially the pitch, yaw, and roll angles of the camera in the established coordinate system in the object space. The rotational matrix $\boldsymbol{M}$ is an orthogonal matrix having the property of $\boldsymbol{M^{-1}} = \boldsymbol{M^T}$ or $\boldsymbol{m_i}^T \boldsymbol{m_j} = \delta_{ij}$. The scaling factor $\lambda = -c / \boldsymbol{m_3}^T (\boldsymbol{X} - \boldsymbol{X_C})$ is a ratio between the principal distance and the projected component of the object space position vector $\boldsymbol{X} - \boldsymbol{X_c}$ on the optical axis in $-\boldsymbol{m_3}$

direction. When an object space point $\boldsymbol{X}$ is on the focal plane $\boldsymbol{m}_3^T(\boldsymbol{X}-\boldsymbol{X}_C)=0$, the scaling factor becomes infinite, i.e., $\lambda=\infty$, which corresponds to the points at infinity on the image (retinal) plane.

The terms δx^1 and δx^2 in Eq. (2.2) are the image coordinate shifts induced by the lens distortion. The lens distortion terms can be modeled by the sum of the radial distortion and decentering distortion [9-10]

$$\delta x^1=\delta x_r^1+\delta x_d^1 \text{ and } \delta x^2=\delta x_r^2+\delta x_d^2, \quad (2.4)$$

where, assuming that the optical axis of the lens is perpendicular to the image plane, we have

$$\begin{aligned}
\delta x_r^1 &= K_1(x^{1\prime}-x_p^1)r^2+K_2(x^{1\prime}-x_p^1)r^4,\\
\delta x_r^2 &= K_1(x^{2\prime}-x_p^2)r^2+K_2(x^{2\prime}-x_p^2)r^4\\
\delta x_d^1 &= P_1[r^2+2(x^{1\prime}-x_p^1)^2]+2P_2(x^{1\prime}-x_p^1)(x^{2\prime}-x_p^2),\\
\delta x_d^2 &= P_2[r^2+2(x^{2\prime}-x_p^2)^2]+2P_1(x^{1\prime}-x_p^1)(x^{2\prime}-x_p^2)\\
r^2 &= (x^{1\prime}-x_p^1)^2+(x^{2\prime}-x_p^2)^2. \quad (2.5)
\end{aligned}$$

Here, K_1 and K_2 are the radial distortion parameters, P_1 and P_2 are the decentering distortion parameters, and $x^{1\prime}$ and $x^{2\prime}$ are the undistorted coordinates in image. When the lens distortion is small, the unknown undistorted coordinates can be approximated by the known distorted coordinates, i.e., $x^{1\prime}\approx x^1$ and $x^{2\prime}\approx x^2$. For large lens distortion, an iterative procedure is employed to determine the appropriate undistorted coordinates to improve the accuracy of the estimate. The following iterative relations are used: $(x^{1\prime})^0=x^1$ and $(x^{2\prime})^0=x^2$, $(x^{1\prime})^{k+1}=x^1+\delta x^1[(x^{1\prime})^k,(x^{2\prime})^k]$ and $(x^{2\prime})^{k+1}=x^2+\delta x^2[(x^{1\prime})^k,(x^{2\prime})^k]$, where the superscripted iteration index k is $k=0,1,2\cdots$.

The collinearity equations Eq. (2.2) can be re-written in the homogenous coordinates in the image plane $\boldsymbol{x}_h=(x^1,x^2,x^3)^T=(x^1,x^2,1)^T$

$$\boldsymbol{A}\boldsymbol{x}_h=\lambda\boldsymbol{M}(\boldsymbol{X}-\boldsymbol{X}_c) \text{ or } \boldsymbol{x}_h=\lambda\boldsymbol{P}(\boldsymbol{X}-\boldsymbol{X}_c), \quad (2.6)$$

where $\boldsymbol{P}=[p_{ij}]=\boldsymbol{A}^{-1}\boldsymbol{M}$ and $\boldsymbol{A}=[a_{ij}]$ is defined as

$$\boldsymbol{A}=\begin{pmatrix} 1 & 0 & -x_p^1+\delta x^1\\ 0 & 1 & -x_p^2+\delta x^2\\ 0 & 0 & -c \end{pmatrix}. \quad (2.7)$$

The terse tensor form of Eq. (2.6) is $a_{ij}x_h^j=\lambda m_{ij}(X^j-X_c^j)$, where the Einstein convention for summation is used. The matrix-form and tensor-form of the collinearity equations are sometimes convenient for mathematical manipulation. Another alternative form of the collinearity equations in the homogenous coordinates is

$$\boldsymbol{x}_h=\lambda\boldsymbol{P}_h\boldsymbol{X}_h, \quad (2.8)$$

where $\boldsymbol{X}_h=(X^1,X^2,X^3,1)^T$ is the homogenous coordinates in the object space, and $\boldsymbol{P}_h=\boldsymbol{A}^{-1}\boldsymbol{M}_h$ and $\boldsymbol{M}_h=(\boldsymbol{M}\ \ -\boldsymbol{M}\boldsymbol{X}_c)$ are 3×4 matrices. Although Eqs. (2.6) and (2.8) are formally written as a linear relation between $\boldsymbol{x}_h$ and $\boldsymbol{X}$ or $\boldsymbol{X}_h$, they are essentially non-linear because not only the lens distortion is a non-linear function of $\boldsymbol{x}$, but also the scaling factor $\lambda=-c/\boldsymbol{m}_3^T(\boldsymbol{X}-\boldsymbol{X}_C)$ is not a constant in general. Nevertheless, because the lens distortion is usually small, its effect can be corrected by using an iterative scheme. Hence, Eqs. (2.6) and (2.8) can be treated as a quasi-linear system at each iteration. Without the lens distortion, the collinearity equations describe the ideal perspective projection. Eq. (2.8) is particularly suitable for utilizing useful results of classical perspective geometry to construct projective geometric invariants.

Furthermore, Eq. (2.2) can be re-written as a form suitable to least-squares estimation for the object space coordinates $\boldsymbol{X}$,

$$\begin{aligned}
\boldsymbol{W}_1^T(\boldsymbol{X}-\boldsymbol{X}_c)&=0\\
\boldsymbol{W}_2^T(\boldsymbol{X}-\boldsymbol{X}_c)&=0
\end{aligned}, \quad (2.9)$$

where $\boldsymbol{W}_1$ and $\boldsymbol{W}_2$ are defined as

$$\begin{aligned}
\boldsymbol{W}_1&=(x^1-x_p^1+\delta x^1)\boldsymbol{m}_3+c\,\boldsymbol{m}_1\\
\boldsymbol{W}_2&=(x^2-x_p^2+\delta x^2)\boldsymbol{m}_3+c\,\boldsymbol{m}_2
\end{aligned}. \quad (2.10)$$

As shown in Fig. 2, the vector $\boldsymbol{W}_1$ is on the plane spanned by the orthogonal unit vectors $\boldsymbol{m}_1$ and $\boldsymbol{m}_3$, while $\boldsymbol{W}_2$ is on a plane spanned by $\boldsymbol{m}_2$ and $\boldsymbol{m}_3$. Geometrically speaking, $\boldsymbol{W}_1^T(\boldsymbol{X}-\boldsymbol{X}_c)=0$ and $\boldsymbol{W}_2^T(\boldsymbol{X}-\boldsymbol{X}_c)=0$ describe two planes normal to $\boldsymbol{W}_1$ and $\boldsymbol{W}_2$ through the optical center. Thus, Eq. (2.9) defines an intersection of these two planes, which is a line through the optical center $\boldsymbol{X}_c$. For a given image point $\boldsymbol{x}=(x^1,x^2)^T$, Eq. (2.9) is not sufficient to determine a point in the object space with the three unknown coordinates $\boldsymbol{X}=(X^1,X^2,X^3)^T$. Hence, extra equations associated with additional cameras and other geometrical constraints should be added for seeking a unique least squares solution of $\boldsymbol{X}$. In contrast to Eq. (2.8), Eq. (2.9) does not include the scaling factor λ.

The collinearity equations Eq. (2.2) contain the camera parameters to be determined by geometric camera calibration. The parameter sets $(\omega,\phi,\kappa,X_c^1,X_c^2,X_c^3)$, (c,x_p^1,x_p^2), and (K_1,K_2,P_1,P_2) in Eq. (2.2) are the exterior orientation, interior orientation, and lens distortion parameters of a camera, respectively. Geometric camera calibration is a key problem in quantitative image-based measurements and a specific topic in both photogrammetry

and computer vision. Here we only briefly address this issue and readers can find the technical details of geometric camera calibration from references. In this paper, we generally assume that the camera is calibrated and a complete set of the orientation parameters and lens distortion parameters of the camera $(\omega,\phi,\kappa,X_c^1,X_c^2,X_c^3,c,x_p^1,x_p^2,K_1,K_2,P_1,P_2)$ is known. Analytical camera calibration techniques utilize the collinearity equations and distortion terms to determine these camera parameters [6-8]. Since Eq. (2.2) is non-linear, iterative methods of least squares estimation have been used as a standard technique for the solution of the collinearity equations in photogrammetry. However, direct recovery of the interior orientation parameters could be problematic and unstable since the normal-equation-matrix of the least squares problem is nearly singular. The singularity of the normal-equation-matrix mainly results from strong correlation between the exterior and interior orientation parameters. In order to reduce the correlation between these parameters and enhance the determinability of (c,x_p,y_p), Fraser [9, 11] suggested the use of multiple camera stations, varying image scales, different camera roll angles and a well-distributed target field in three dimensions. Nevertheless, the multiple-station, multiple-image method for camera calibration is not easy to use in many engineering and scientific applications like wind tunnel testing where optical access for cameras is limited and the positions of cameras are fixed. Abdel-Aziz and Karara [12] proposed a simple linear method for camera calibration, Direct Linear Transformation (DLT). Scientists in computer vision and robotics have developed various camera calibration schemes to achieve a fast calibration with an acceptable accuracy (a lower accuracy for a photogrammetric application). Tsai's two-step method [13] is representative in computer vision, which uses a radial alignment constraint to obtain a linear least squares solution for a subset of the calibration parameters, whereas the rest of the parameters including the radial distortion parameter are estimated by an iterative scheme. By circumventing the singularity problem, Liu et al. [14] developed a robust optimization method for single-image, automatic camera calibration to determine the interior and exterior orientation parameters and lens distortion parameters plus the pixel spacing ratio.

3. Projective Developable Conical Surface Containing 3D Curve

In this section, we introduce the concept of projective developable conical surface and show how to reconstruct this surface containing a 3D curve from a single image. In principle, a 3D curve in the object space cannot be completely recovered from a single image since information in one dimension is lost in the imaging process. Nevertheless, using a calibrated camera, a projective conical developable surface on which a 3D curve lies can be reconstructed. When two calibrated cameras are used, the 3D curve can be uniquely determined as an intersection of two different projective conical developable surfaces. Furthermore, a 3D surface can be reconstructed as an envelope of a family of the projective developable conical surfaces obtained from images taken at different viewing angles. The motion field of the 3D curve can be obtained from a time sequence of the curve.

Generating Projective Developable Conical Surface

Consider a 3D simple curve C in the object space, and its projection to the image plane and a plane P normal to the optical axis (parallel to the image plane), as shown Fig. 3. The collinearity equations Eq. (2.6) are written as

$$\boldsymbol{X} - \boldsymbol{X}_c = \lambda^{-1}\overline{\boldsymbol{P}}\,\boldsymbol{x}_h, \tag{3.1}$$

where $\overline{\boldsymbol{P}} = \boldsymbol{P}^{-1} = [\,\overline{p}_{ij}\,] = \boldsymbol{M}^{-1}\boldsymbol{A} = \boldsymbol{M}^{T}\boldsymbol{A}$. When the camera parameters and the scaling factor are constant and the lens distortion is fixed, differentiating Eq. (3.1) yields

$$d\boldsymbol{X} = \lambda^{-1}\overline{\boldsymbol{P}}_{32}\,d\boldsymbol{x}, \tag{3.2}$$

where $d\boldsymbol{X} = (dX^1, dX^2, dX^3)^T$, $d\boldsymbol{x} = (dx^1, dx^2)^T$, and

$$\overline{\boldsymbol{P}}_{32} = \begin{pmatrix} \overline{p}_{11} & \overline{p}_{12} \\ \overline{p}_{21} & \overline{p}_{22} \\ \overline{p}_{31} & \overline{p}_{32} \end{pmatrix}.$$

A constraint imposed on Eq. (3.2) is $\boldsymbol{m}_3^T d\boldsymbol{X} = 0$, indicating that Eq. (3.2) actually describes the projection C_P of the 3D curve C on the plane P orthogonal to the optical axis direction or $\boldsymbol{m}_3$. This constraint is equivalent to the constancy condition of the scaling factor $\lambda = -c/\boldsymbol{m}_3^T(\boldsymbol{X} - \boldsymbol{X}_C)$ since the differential $d\lambda = c\,\boldsymbol{m}_3^T d\boldsymbol{X} / [\boldsymbol{m}_3^T(\boldsymbol{X} - \boldsymbol{X}_c)]^2$ shows $\boldsymbol{m}_3^T d\boldsymbol{X} = 0 \Leftrightarrow d\lambda = 0$. In fact, the constraint $\lambda = -c/\boldsymbol{m}_3^T(\boldsymbol{X} - \boldsymbol{X}_c) = const.$ defines the plane orthogonal to the optical axis direction or $\boldsymbol{m}_3$. As shown in Fig. 3, the projected curve C_P on the plane P can be reconstructed from the image and then the developable conical surface D containing the 3D curve C can be generated.

The arc length element of the projected curve C_P on the plane P is

$$dS_{C_P} = |\,d\boldsymbol{X}\,| = \lambda^{-1}\,|\,\overline{\boldsymbol{P}}_{32}\,\boldsymbol{t}\,|\,ds, \tag{3.3}$$

where $\boldsymbol{t} = d\boldsymbol{x}/ds$ and $ds = |\,d\boldsymbol{x}\,|$ are the unit tangent vector and arc length element of the image of the 3D curve C in the image plane, respectively. Thus, the unit tangent vector of the projected curve C_P on the plane P is

$$\boldsymbol{T}_{C_P} = \frac{d\boldsymbol{X}}{dS_{C_P}} = \frac{\overline{\boldsymbol{P}}_{32}\,\boldsymbol{t}}{|\,\overline{\boldsymbol{P}}_{32}\,\boldsymbol{t}\,|}\ . \tag{3.4}$$

Note that the unit tangent vector $\boldsymbol{T}_{C_P}$ is independent of the scaling factor λ. The curvature vector of the projected curve C_P on the plane P can be obtained by differentiating Eq. (3.4) with respect to the arc length S_{C_P}

$$\boldsymbol{K}_{C_P} = \frac{d\boldsymbol{T}_{C_P}}{dS_{C_P}} = \frac{\lambda}{|\overline{\boldsymbol{P}}_{32}\boldsymbol{t}|^2}(\overline{\boldsymbol{P}}_{32}\boldsymbol{k} - \boldsymbol{T}_{C_P}\frac{d|\overline{\boldsymbol{P}}_{32}\boldsymbol{t}|}{ds}), \quad (3.5)$$

where $\boldsymbol{k} = d\boldsymbol{t}/ds = d^2\boldsymbol{x}/ds^2$ is the curvature vector of the curve image in the image plane. The curvature vector $\boldsymbol{k}$ can be expressed as $\boldsymbol{k} = \kappa_c \boldsymbol{n}$, where κ_c and $\boldsymbol{n} = \boldsymbol{k}/|\boldsymbol{k}|$ are the curvature and the unit normal vector of the curve image in the image plane, respectively. Furthermore, we prove

$$\frac{d|\overline{\boldsymbol{P}}_{32}\boldsymbol{t}|}{ds} = \frac{(\overline{\boldsymbol{P}}_{32}\boldsymbol{k})^T(\overline{\boldsymbol{P}}_{32}\boldsymbol{t})}{|\overline{\boldsymbol{P}}_{32}\boldsymbol{t}|}. \quad (3.6)$$

Hence, Eq. (3.5) becomes

$$\boldsymbol{K}_{C_P} = \frac{\kappa_c\lambda}{|\overline{\boldsymbol{P}}_{32}\boldsymbol{t}|^2}[\overline{\boldsymbol{P}}_{32}\boldsymbol{n} - \boldsymbol{T}_{C_P}\frac{(\overline{\boldsymbol{P}}_{32}\boldsymbol{n})^T(\overline{\boldsymbol{P}}_{32}\boldsymbol{t})}{|\overline{\boldsymbol{P}}_{32}\boldsymbol{t}|}]. \quad (3.7)$$

The curvature of the projected curve C_P on the plane P is $\kappa_{C_P} = \boldsymbol{K}_{C_P} \bullet \boldsymbol{N}_{C_P}$, where $\boldsymbol{N}_{C_P} = \boldsymbol{K}_{C_P}/|\boldsymbol{K}_{C_P}|$ is the principal normal vector of the projected curve C_P. Thus, the ratio between the curvatures κ_{C_P} on the plane P and κ_c on the image plane is

$$\frac{\kappa_{C_P}}{\kappa_c} = \frac{\lambda}{|\overline{\boldsymbol{P}}_{32}\boldsymbol{t}|^2}[\overline{\boldsymbol{P}}_{32}\boldsymbol{n} - \boldsymbol{T}_{C_P}\frac{(\overline{\boldsymbol{P}}_{32}\boldsymbol{n})^T(\overline{\boldsymbol{P}}_{32}\boldsymbol{t})}{|\overline{\boldsymbol{P}}_{32}\boldsymbol{t}|}] \bullet \boldsymbol{N}_{C_P}. \quad (3.8)$$

Clearly, Eq. (3.8) indicates that κ_{C_P}/κ_c is proportional to the scaling factor λ.

After the unit tangent vector $\boldsymbol{T}_{C_P}$ is obtained from the image, the projected curve C_P on the plane P is readily reconstructed by

$$\boldsymbol{X}_{C_P} = \boldsymbol{X}_{C_P 0} + \int_0^{S_{C_P}} \boldsymbol{T}_{C_P}(S_{C_P})dS_{C_P}. \quad (3.9)$$

The initial position $\boldsymbol{X}_{C_P 0}$ on the projected curve C_P, in the object space is often chosen at the end point of the curve. Eq. (3.1) gives $\boldsymbol{X}_{C_P 0} - \boldsymbol{X}_c = \lambda^{-1}\overline{\boldsymbol{P}}\,\boldsymbol{x}_{h0}$, where $\boldsymbol{x}_{h0} = (x_0^1, x_0^2, 1)^T$ is the homogenous coordinates of the corresponding image point to $\boldsymbol{X}_{C_P 0}$. Substituting Eqs. (3.3) and (3.4) into Eq. (3.9) yields a ray vector directing from the optical center $\boldsymbol{X}_c$ to a point $\boldsymbol{X}_{C_P}$ on the projected curve C_P

$$\boldsymbol{X}_{C_P} - \boldsymbol{X}_c = \lambda^{-1}(\overline{\boldsymbol{P}}\,\boldsymbol{x}_{h0} + \int_0^s \overline{\boldsymbol{P}}_{32}\boldsymbol{t}\,ds). \quad (3.10)$$

A family of the projective rays through the optical center $\boldsymbol{X}_c$ given by Eq. (3.10) generates a projective developable conical surface D that contains the 3D curve C. The tangent plane on the developable conical surface D is given by

$$(\boldsymbol{X} - \boldsymbol{X}_c) \bullet \boldsymbol{N}_D(s) = 0, \quad (3.11)$$

where $\boldsymbol{N}_D(s) = \boldsymbol{T}_{C_P} \times (\boldsymbol{X}_{C_P} - \boldsymbol{X}_c)/|\boldsymbol{T}_{C_P} \times (\boldsymbol{X}_{C_P} - \boldsymbol{X}_c)|$ is the unit normal vector to the tangent plane on the developable surface, which is independent of the scaling factor. Eq. (3.11) describes a single-parameter family of the tangent planes where the parameter is the arc length s of the curve in the image plane. The projective conical developable surface, the envelope generated by the family of the tangent planes, is given by a system of Eq. (3.11) and Eq. (3.12) [15]

$$(\boldsymbol{X} - \boldsymbol{X}_c) \bullet d\boldsymbol{N}_D(s)/ds = 0. \quad (3.12)$$

Thus, the projective developable conical surface and associated geometric quantities such as the curvature, tangent vector and normal vector in the 3D object space can be obtained by using measured image quantities given the camera parameters.

Reconstructing 3D curve and Surface

From a single image, we are able to reconstruct the projective conical developable surface containing the 3D curve C rather than the 3D curve itself. Nevertheless, when two calibrated cameras are used, as shown in Fig. 4, the 3D curve C can be uniquely determined by intersecting the two projective developable conical surfaces associated with the different cameras. Interestingly, the developable conical surface intersection method for determining the 3D curve only requires knowing the correspondence of one distinguished point such as an end point of the curve.

Furthermore, the developable conical surfaces can be used to reconstruct a 3D surface in the object space. As shown in Fig. 5, the developable conical surface containing the contour of the 3D surface can be constructed. Here the contour is a set of points on the 3D surface at which the surface normal is also the normal of the developable conical surface. When the camera is moved to a number of known positions through a rotational and translational transformation (rigid-body motion), a family of the developable conical surfaces can be obtained. The 3D surface is generated as an envelope of the family of the conical surfaces. Instead of moving the camera, the 3D surface can be rotated around a fixed axis such that a family of the conical surfaces can be obtained using a camera at a fixed position and viewing angle. From a computational viewpoint, this method may not be the most efficient since the intersection and envelope of the developable conical surfaces has to be determined. However, this method is to great extent immune from the ambiguous correspondence problem in stereovision.

Recovering Motion Field of 3D Curve

After two or more 3D curves in the object space at successive instants are reconstructed, we can estimate the motion field $\boldsymbol{U}(\boldsymbol{X})$ of the 3D curve that is defined as

$$\boldsymbol{U}(\boldsymbol{X}) = \frac{d\boldsymbol{X}}{dt}. \quad (3.13)$$

The curve is given by $\boldsymbol{X} = \boldsymbol{X}[S(t),t]$, where t is time and $S(t)$ is the arc length of the curve in the object space. Measurements give the temporal and spatial difference between two curves at two successive instants t_1 and t_2 (the time interval $\Delta t = t_2 - t_1$ is small)

$$\Delta_{St}\boldsymbol{X} = \boldsymbol{X}[S(t_2),t_2] - \boldsymbol{X}[S(t_1),t_1]. \quad (3.14)$$

Reconstruction of the motion field of the 3D curve from $\Delta_{St}\boldsymbol{X}$ is a non-trivial problem since the point correspondence between two sequential images is not known without using distinct targets on the curve especially for an elastic curve experiencing large and complicated deformation.

The motion field of the curve is constrained by the underlying physical mechanisms behind the motion and deformation of the curve. In general, reconstructing the motion field is formulated as an optimization problem of the functional

$$J[\boldsymbol{U}(\boldsymbol{X})] = \| \Delta_{St}\boldsymbol{X} - \boldsymbol{U}(\boldsymbol{X})\Delta t \| \rightarrow min \quad (3.15)$$

subject to relevant physical and geometric constraints

$$G_i[\boldsymbol{U}(\boldsymbol{X})] = 0, \quad (i = 1,2,\cdots) \quad (3.16)$$

and the suitable boundary conditions. Without the sufficient constraints, the solution to the optimization problem may not be unique. Also, the imposed physical constraints serve as a bridge connecting image-based measurements with the physical quantities in a specific problem being studied.

In the simplest case in which the curve is rigid, the rigid-body motion field is expressed as

$$\boldsymbol{U}(\boldsymbol{X}) = \boldsymbol{U}_0 + \boldsymbol{\Omega}_0 \times (\boldsymbol{X} - \boldsymbol{X}_0), \quad (3.17)$$

where $\boldsymbol{U}_0$ and $\boldsymbol{\Omega}_0$ are the constant translation velocity and angular velocity, respectively, and $\boldsymbol{X}_0$ is the rotational center of the curve. Because $\boldsymbol{U}_0$ and $\boldsymbol{\Omega}_0$ together contain only six unknown constants, it is easier to solve the optimization problem. A slightly complicated case is that the curve is stretched in three fixed directions in addition to the constant translation and rotation. In this case, three stretching constants are added, and thus the total number of the unknowns in the optimization problem is nine. Next, we consider a highly deformable material line convected in an incompressible and irrotational flow. In this case, the physical constraints are the solenoidal and irrotational conditions [16]

$$\nabla \bullet \boldsymbol{U}(\boldsymbol{X}) = 0 \text{ and } \nabla \times \boldsymbol{U}(\boldsymbol{X}) = 0. \quad (3.18)$$

A vortex-filament in an incompressible and irrotational flow is an interesting example since the filament driven by not only mean flow, but also self-induction is no longer passive and the motion field is directly related to the geometric features of the filament. In this case, the induced motion velocity of the filament is proportional to the curvature κ of the filament along the binormal direction vector $\boldsymbol{B}$ [17]

$$\boldsymbol{U}(\boldsymbol{X}) \propto \kappa \boldsymbol{B}. \quad (3.19)$$

Overall, the physical constraints for a specific application are necessary for recovering the correct motion field and associated physical properties of the 3D curve.

4. Perspective Projection under Surface Constraint

In general, mapping between a point in the 3D object space and the corresponding image point is not one-to-one. Nevertheless, as shown in Fig. 6, under a given surface constraint, a point on the surface has the one-to-one correspondence to the image point. In this section, we discuss the geometric relationship between the surface in the object space and the image plane. This topic is closely related to some applications in experimental fluid mechanics and aerodynamics such as reconstruction of complex flow topology from images of surface oil visualization and laser-sheet-induced fluorescence visualization. Consider a surface in the object space given by

$$X^3 = F(X^1, X^2). \quad (4.1)$$

When Eq. (4.1) is imposed on Eq. (2.9) as a surface constraint, the perspective projection transformation Eq. (2.9) is reduced to

$$\begin{aligned}(w_{11}w_{23} - w_{13}w_{21})X^1 + (w_{12}w_{23} - w_{13}w_{22})X^2 \\ = w_{23}\boldsymbol{W_1}^T\boldsymbol{X}_c - w_{13}\boldsymbol{W_2}^T\boldsymbol{X}_c \\ w_{11}X^1 + w_{12}X^2 + w_{13}F(X^1, X^2) = \boldsymbol{W_1}^T\boldsymbol{X}_c, \end{aligned} \quad (4.2)$$

where w_{ij} ($i = 1,2$ and $j = 1,2,3$) are the elements of the vectors $\boldsymbol{W_1} = (w_{11}, w_{12}, w_{13})^T$ and $\boldsymbol{W_2} = (w_{21}, w_{22}, w_{23})^T$. For the given surface equation $X^3 = F(X^1, X^2)$ and the known camera parameters, the coordinates $(X^1, X^2)^T$ can be obtained from the image coordinates $\boldsymbol{x} = (x^1, x^2)^T$ by numerically solving Eq. (4.2). Thus, the coordinates $\boldsymbol{X} = (X^1, X^2, X^3)^T$ in the object space can be symbolically expressed as a function of the image coordinates $\boldsymbol{x} = (x^1, x^2)^T$, that is,

$$\boldsymbol{X} = \boldsymbol{f_S}(\boldsymbol{x}). \quad (4.3)$$

In fact, Eq. (4.3) is a parametric representation of the surface using the image coordinates $\boldsymbol{x} = (x^1, x^2)^T$ as the parameters. Generally, the function $\boldsymbol{f_S}(\boldsymbol{x})$ cannot be written as a closed-form solution except in some special cases such as a plane and a cylindrical surface.

Differentiating Eq. (2.9), we have

$$\begin{aligned} d\boldsymbol{W_1}^T\boldsymbol{X} + \boldsymbol{W_1}^T d\boldsymbol{X} = d\boldsymbol{W_1}^T\boldsymbol{X}_c \\ d\boldsymbol{W_2}^T\boldsymbol{X} + \boldsymbol{W_2}^T d\boldsymbol{X} = d\boldsymbol{W_2}^T\boldsymbol{X}_c. \end{aligned} \quad (4.4)$$

When the lens distortion is fixed, $d\boldsymbol{W_1}^T = dx^1\boldsymbol{m_3}^T$ and $d\boldsymbol{W_2}^T = dx^2\boldsymbol{m_3}^T$ hold. Then, substitution of

$dX^3 = (\partial F/\partial X^1)dX^1 + (\partial F/\partial X^2)dX^2$ into Eq. (4.4) yields

$$\begin{pmatrix} dX^1 \\ dX^2 \end{pmatrix} = \boldsymbol{m}_3^T(\boldsymbol{X}_c - \boldsymbol{f}_S)Q^{-1}\begin{pmatrix} dx^1 \\ dx^2 \end{pmatrix}, \quad (4.5)$$

where

$$Q = \begin{pmatrix} w_{11} + w_{13}\,\partial F/\partial X^1 & w_{12} + w_{13}\,\partial F/\partial X^2 \\ w_{21} + w_{23}\,\partial F/\partial X^1 & w_{22} + w_{23}\,\partial F/\partial X^2 \end{pmatrix}. \quad (4.6)$$

Furthermore, the differential dX^3 can be expressed as a function of the image coordinates $d\boldsymbol{x} = (dx^1, dx^2)^T$

$$dX^3 = (dF/dx^1)dx^1 + (dF/dx^2)dx^2, \quad (4.7)$$

where

$$\frac{dF}{dx^\alpha} = \frac{\partial F}{\partial X^1}\frac{\partial X^1}{\partial x^\alpha} + \frac{\partial F}{\partial X^2}\frac{\partial X^2}{\partial x^\alpha}. \ (\alpha = 1,2) \quad (4.8)$$

Combining Eqs. (4.5) and (4.7), we have

$$d\boldsymbol{X} = \boldsymbol{m}_3^T(\boldsymbol{X}_c - \boldsymbol{f}_S)\overline{Q}\,d\boldsymbol{x}, \quad (4.9)$$

where

$$\overline{Q} = \begin{pmatrix} Q^{-1} \\ (\frac{dF}{dx^1}, \frac{dF}{dx^2})/\boldsymbol{m}_3^T(\boldsymbol{X}_c - \boldsymbol{f}_S) \end{pmatrix}. \quad (4.10)$$

Eq. (4.9) provides a fundamental relation between the differentials $d\boldsymbol{X}$ on the surface and $d\boldsymbol{x}$ on the image plane. The matrix $\overline{Q}$ is a function of the image coordinates, the camera parameters, and the geometric properties of the given surface.

On the other hand, we notice

$$d\boldsymbol{X} = (\partial\boldsymbol{X}/\partial x^1)dx^1 + (\partial\boldsymbol{X}/\partial x^2)dx^2. \quad (4.11)$$

From Eqs. (4.9) and (4.11), we obtain the following equality

$$(\partial\boldsymbol{X}/\partial x^1, \partial\boldsymbol{X}/\partial x^2) = \boldsymbol{m}_3^T(\boldsymbol{X}_c - \boldsymbol{f}_S)\overline{Q}. \quad (4.12)$$

The element dS of the arc length of a curve on the surface can be determined from Eqs. (4.11) and (4.12) from the image coordinates. We know

$$dS^2 = |d\boldsymbol{X}| = g_{\alpha\beta}\,dx^\alpha dx^\beta, \quad (4.13)$$

where

$$g_{\alpha\beta} = \frac{\partial\boldsymbol{X}}{\partial x^\alpha} \bullet \frac{\partial\boldsymbol{X}}{\partial x^\beta} \quad (\alpha, \beta = 1,2) \quad (4.14)$$

is the so-called metric tensor in classical differential geometry [18]. The summation convention is used in Eqs. (4.13) and (4.14). The quadratic differential form Eq. (4.13) is the first fundamental form of the surface in which the image coordinates are the parametric variables. In the case of the perspective projection transformation, $g_{\alpha\beta}$ may be properly named as the perspective metric tensor that is a function of the image coordinates, the camera parameters, and the properties of the given surface.

The first fundamental form Eq. (4.13) allows us to measure the basic geometric quantities on the surface in the 3D object space from the image quantities. Consider a curve on the image plane given by a parametric form $\boldsymbol{x}(t) = (x^1(t), x^2(t))^T$ and the corresponding 3D curve on the surface $\boldsymbol{X}(t) = \boldsymbol{X}(\boldsymbol{x}(t)) = \boldsymbol{f}_S(\boldsymbol{x}(t))$, where t is a parameter (e.g. time). The length of an arc bounded the points corresponding to the parametric values $t = t_0$ and $t = t_1$ is

$$S = \int_{t_0}^{t_1} [\,g_{\alpha\beta}(dx^\alpha/dt)(dx^\beta/dt)\,]^{1/2}dt. \quad (4.15)$$

The angle of two 3D curves at the intersecting point on the surface can be calculated based on the image quantities. Consider two image curves $\boldsymbol{x}(t) = (x^1(t), x^2(t))^T$ and $\boldsymbol{x}(t) = (x^{1+}(t), x^{2+}(t))^T$. The tangential vectors of the two 3D curves on the surface are $d\boldsymbol{X}(x^1(t), x^2(t))/dt = \partial\boldsymbol{X}/\partial x^\alpha\, dx^\alpha/dt$ and $d\boldsymbol{X}(x^{1+}(t), x^{2+}(t))/dt = \partial\boldsymbol{X}/\partial x^{\alpha+}\, dx^{\alpha+}/dt$. Thus, the angle γ of intersection is

$$\cos\gamma = \frac{g_{\alpha\beta}(dx^\alpha/dt)(dx^{\beta+}/dt)}{\sqrt{g_{\alpha\beta}(dx^\alpha/dt)(dx^\beta/dt)}\sqrt{g_{\alpha\beta}(dx^{\alpha+}/dt)(dx^{\beta+}/dt)}}. \quad (4.16)$$

The area of a domain H on the surface can be expressed in the image coordinates

$$A(H) = \iint_U \sqrt{g}\,dx^1 dx^2, \quad (4.17)$$

where U is the domain in the image (x^1, x^2) plane corresponding to the domain H on the surface in the object space and g is the determinant $g = |\,g_{\alpha\beta}\,|$.

Example 1: Plane

The plane constraint is a simple, but very useful case in which the vector function $\boldsymbol{f}_S(\boldsymbol{x})$, the matrices Q and $\overline{Q}$ can be explicitly expressed as a function of the known camera parameters and the measured image coordinates. Many aerodynamic flow structures are observed on a plane or a near-planar surface. Planar laser sheet flow visualization is just a typical case of the plane constraint. In addition, a polyhedron consists of a number of the planar faces. Consider a plane in the object space

$$X^3 = a_1 X^1 + a_2 X^2 + a_3. \quad (4.18)$$

This plane is defined by the vector $\boldsymbol{a} = (a_1, a_2, a_3)^T$ related to the normal vector of the plane. In this case, the matrix Q in Eq. (4.6) is

$$Q = \begin{pmatrix} w_{11} + w_{13}\,a_1 & w_{12} + w_{13}\,a_2 \\ w_{21} + w_{23}\,a_1 & w_{22} + w_{23}\,a_2 \end{pmatrix}. \quad (4.19)$$

The function $\boldsymbol{f}_S(\boldsymbol{x})$ in Eq. (4.3) has a closed-form solution

$$\boldsymbol{f}_S(\boldsymbol{x}) = \begin{pmatrix} Q^{-1}\boldsymbol{l} \\ \boldsymbol{a}^T \begin{pmatrix} Q^{-1}\boldsymbol{l} \\ 1 \end{pmatrix} \end{pmatrix}, \tag{4.20}$$

where

$$\boldsymbol{l} = \begin{pmatrix} \boldsymbol{W_1}^T \boldsymbol{X_c} - w_{13}\, a_3 \\ \boldsymbol{W_2}^T \boldsymbol{X_c} - w_{23}\, a_3 \end{pmatrix}. \tag{4.21}$$

Now the matrix $\overline{Q}$ in Eq. (4.10) is

$$\overline{Q} = \begin{pmatrix} Q^{-1} \\ (a_1, a_2) Q^{-1} \end{pmatrix}. \tag{4.22}$$

Example 2: Cylindrical Surface

A cylindrical surface is another case where $\boldsymbol{f}_S(\boldsymbol{x})$, Q and $\overline{Q}$ can be explicitly expressed. For the sake of convenience, a transformation from the Cartesian coordinate system to the cylindrical coordinate system is used, i.e.,

$$\boldsymbol{X} = (X^1, X^2, X^3)^T = (\rho\cos\varphi, \rho\sin\varphi, z)^T, \tag{4.23}$$

where ρ is the radial coordinate, φ is the polar angle, and z is the axial coordinate. The differential $d\boldsymbol{X}$ is

$$d\boldsymbol{X} = \begin{pmatrix} \cos\varphi & -\rho\sin\varphi & 0 \\ \sin\varphi & \rho\cos\varphi & 0 \\ 0 & 0 & 1 \end{pmatrix} \begin{pmatrix} d\rho \\ d\varphi \\ dz \end{pmatrix}. \tag{4.24}$$

For a cylindrical surface constraint $\rho = \rho_0 = const.$, solving Eq. (2.9) for φ and z, we have $\boldsymbol{f}_S(\boldsymbol{x})$ as a function of the image coordinates and camera parameters

$$\boldsymbol{f}_S(\boldsymbol{x}) = (\rho_0 \cos\varphi, \rho_0 \sin\varphi, z)^T, \tag{4.25}$$

where

$$\cos\varphi = \frac{b_1 b_3 \pm \sqrt{b_1^2 b_2^2 + b_2^4 - b_2^2 b_3^2}}{b_1^2 + b_2^2},$$

$$\sin\varphi = \frac{b_2 b_3 \pm \sqrt{b_2^2 b_1^2 + b_1^4 - b_1^2 b_3^2}}{b_1^2 + b_2^2},$$

$$z = w_{13}^{-1}(w_{11}\rho_0 \cos\varphi + w_{12}\ \rho_0 \sin\varphi - \boldsymbol{W_1}^T \boldsymbol{X}_c),$$

$$b_1 = \rho_0(w_{11}w_{23} - w_{21}w_{13}),$$

$$b_2 = \rho_0(w_{12}w_{23} - w_{22}w_{13}),$$

$$b_3 = w_{23}\boldsymbol{W_1}^T \boldsymbol{X_c} - w_{13}\boldsymbol{W_2}^T \boldsymbol{X_c}.$$

There are two solutions for $\boldsymbol{f}_S(\boldsymbol{x})$, which are corresponding to two intersecting points between a perspective ray and the cylinder. For a non-transparent solid surface, a camera only sees one intersecting point at the surface facing the camera and hence $\boldsymbol{f}_S(\boldsymbol{x})$ is one-to-one. The differentials in the cylindrical coordinate system are related to the image coordinate differentials by the following relation

$$d(\varphi, z)^T = \boldsymbol{m_3}^T(\boldsymbol{X_c} - \boldsymbol{f}_S) Q^{-1} d\boldsymbol{x}, \tag{4.26}$$

where

$$Q = \begin{pmatrix} w_{12}\rho_0 \cos\varphi - w_{11}\rho_0 \sin\varphi & w_{13} \\ w_{22}\rho_0 \cos\varphi - w_{21}\rho_0 \sin\varphi & w_{23} \end{pmatrix}. \tag{4.27}$$

Another differential is $d\rho = 0$. Note that the expressions of $\boldsymbol{f}_S(\boldsymbol{x})$, Q and $\overline{Q}$ for a spherical surface can be also analytically derived, but they are so tedious that we do not present them here.

5. Perspective Projection of Motion Field Constrained on Surface

After discussing the geometric relationship between a surface in the object space and the image plane, we study kinematics under the surface constraint, that is, the perspective projection of a motion field on a surface. Consider a dynamical system

$$\frac{d\boldsymbol{X}}{dt} = \boldsymbol{U}(\boldsymbol{X}), \tag{5.1}$$

where $\boldsymbol{U}(\boldsymbol{X}) = (U_1, U_2, U_3)^T$ is a motion field in the 3D object space and t is time. A surface constraint imposed on the motion field Eq. (5.1) is

$$X^3 = F(X^1, X^2). \tag{5.2}$$

Under this surface constraint, $\boldsymbol{U}(\boldsymbol{X})$ should be parallel to the surface, which obeys the orthogonality condition

$$\boldsymbol{N}_s \bullet \boldsymbol{U}(\boldsymbol{X}) = 0, \tag{5.3}$$

where $\boldsymbol{N}_s = (\partial F/\partial X^1, \partial F/\partial X^2, -1)^T$ is the normal vector of the surface. Under the surface constraint Eq. (5.2), Eq. (5.1) is effectively reduced to a 2D system

$$\frac{d}{dt}\begin{pmatrix} X^1 \\ X^2 \end{pmatrix} = \begin{pmatrix} U_1[X^1, X^2, F(X^1, X^2)] \\ U_2[X^1, X^2, F(X^1, X^2)] \end{pmatrix}. \tag{5.4}$$

In fact, Eq. (5.4) describes an orthographic projection of the motion field Eq. (5.1) onto the plane (X^1, X^2). From Eq. (4.5), the dynamical system in the image plane, which is corresponding to Eq. (5.4), is

$$\boldsymbol{u} = \frac{d}{dt}\begin{pmatrix} x^1 \\ x^2 \end{pmatrix} = \frac{Q}{\boldsymbol{m_3}^T(\boldsymbol{X_c} - \boldsymbol{f}_S)} \begin{pmatrix} U_1[\boldsymbol{f}_S(\boldsymbol{x})] \\ U_2[\boldsymbol{f}_S(\boldsymbol{x})] \end{pmatrix}. \tag{5.5}$$

We call $\boldsymbol{u} = d\boldsymbol{x}/dt = d/dt(x^1, x^2)^T$ the optic flow in the image plane. The optic flow, a term first used in computer vision, is defined as the velocity field in the image plane that transforms one image into the next image in a sequence. If Eq. (4.2) gives a one-to-one topological mapping (homeomorphism): $(x^1, x^2) \mapsto (X^1, X^2)$, the topological structure of the dynamical system Eq. (5.5) in the image plane is equivalent to that of Eq. (5.4) on the surface in the object space when Q has the full rank of 2 and $\boldsymbol{m_3}^T(\boldsymbol{X_c} - \boldsymbol{f}_S)$ is not zero. Figure 6 illustrates this point. The problem is to recover two components of the motion field $(U_1, U_2)^T$ using Eq. (5.5) from the measured

optic flow $\boldsymbol{u} = d\boldsymbol{x}/dt$, while the third component U_3 is readily obtained from the orthogonal condition Eq. (5.3).

In the above analysis, we do not specify the motion field $\boldsymbol{U}(\boldsymbol{X})$, which could be a limiting viscous flow field, an oil-film motion field driven by skin friction, or a particle motion field driven by a potential force (e.g. gravity and electromagnetic force). The physical constraints on $\boldsymbol{U}(\boldsymbol{X})$, which are different in different cases, are necessary to reduce the number of unknowns. For instance, an incompressible flow must obey the continuity equation

$$\nabla \bullet \boldsymbol{U}(\boldsymbol{X}) = 0, \tag{5.6}$$

where $\nabla = (\partial/\partial X^1, \partial/\partial X^2, \partial/\partial X^3)^T$ is the Laplace operator. Differentiating Eq. (5.3) with respect to X^3, we have

$$\frac{\partial U_3}{\partial X^3} = \frac{\partial F}{\partial X^1}\frac{\partial U_1}{\partial X^3} + \frac{\partial F}{\partial X^2}\frac{\partial U_2}{\partial X^3}. \tag{5.7}$$

Substitution of Eq. (5.7) into Eq. (5.6) yields a constraint on $(U_1, U_2)^T$ for an incompressible flow field,

$$\left(\frac{\partial}{\partial X^1} + \frac{\partial F}{\partial X^1}\frac{\partial}{\partial X^3}\right)U_1 + \left(\frac{\partial}{\partial X^2} + \frac{\partial F}{\partial X^2}\frac{\partial}{\partial X^3}\right)U_2 = 0. \tag{5.8}$$

In general, it is more difficult to directly obtain a global solution of Eq. (5.5) for the motion field $(U_1, U_2)^T$. Instead, we can seek a localized solution of Eq. (5.5) in a sufficiently small area. In a neighborhood of a point $\boldsymbol{X_0}$, the motion field $(U_1, U_2)^T$ can be expanded as a linear function of $\boldsymbol{X}$

$$U_i(\boldsymbol{X}) = e_{i0} + (e_{i1}, e_{i2}, e_{i3})(\boldsymbol{X} - \boldsymbol{X_0}), \ (i = 1,2) \tag{5.9}$$

where $e_{i0} = U_i(\boldsymbol{X_0})$ are the local velocity components and $e_{ij} = \partial U_i(\boldsymbol{X_0})/\partial \boldsymbol{X}^j$ $(j = 1,2,3)$ are the local deformation components. Hence, the localized form of Eq. (5.5) is written as

$$\boldsymbol{Du} = \frac{d}{dt}\begin{pmatrix} x^1 \\ x^2 \end{pmatrix} - \frac{Q}{\boldsymbol{m_3}^T(\boldsymbol{X_c} - \boldsymbol{f_S})} \times \begin{pmatrix} e_{10} + (e_{11}, e_{12}, e_{13})[\boldsymbol{f_S}(\boldsymbol{x}) - \boldsymbol{f_S}(\boldsymbol{x_0})] \\ e_{20} + (e_{21}, e_{22}, e_{23})[\boldsymbol{f_S}(\boldsymbol{x}) - \boldsymbol{f_S}(\boldsymbol{x_0})] \end{pmatrix} = 0. \tag{5.10}$$

The unknowns e_{i0} and e_{ij}, can be determined by minimizing the norm $||\boldsymbol{Du}||$, i.e.,

$$||\boldsymbol{Du}|| \to min. \tag{5.11}$$

At the final stage, the global motion field on the surface is reconstructed from the local motion fields.

In an incompressible flow, the localized constraint Eq. (5.8) is

$$e_{11} + e_{13}\frac{\partial F}{\partial X^1} + e_{22} + e_{23}\frac{\partial F}{\partial X^2} = 0. \tag{5.12}$$

Furthermore, for the irrotational motion field on a solid surface where the vorticity vanishes, i.e., $\boldsymbol{\omega} = \nabla \times \boldsymbol{U}(\boldsymbol{X}) = 0$, three constraints are

$$U_1\frac{\partial^2 F}{\partial X^1 \partial X^2} + e_{12}\frac{\partial F}{\partial X^1} + U_2\frac{\partial^2 F}{\partial X^2 \partial X^2} + e_{22}\frac{\partial F}{\partial X^2} - e_{23} = 0,$$
$$U_1\frac{\partial^2 F}{\partial X^1 \partial X^1} + e_{11}\frac{\partial F}{\partial X^1} + U_2\frac{\partial^2 F}{\partial X^2 \partial X^1} + e_{21}\frac{\partial F}{\partial X^2} - e_{31} = 0,$$
$$e_{21} - e_{12} = 0. \tag{5.13}$$

Hence, for an incompressible, irrotational motion field, eight unknowns in Eq. (5.10) are reduced to four unknowns after these constraints are imposed. At the critical points, the velocity vanishes, i.e., $e_{i0} = U_i(\boldsymbol{X_0}) = 0$. The local topological structures of the motion field at the critical points are determined by the deformation coefficients e_{ij} [19].

The above method for calculating the local motion field is applicable to both discrete random particle patterns (e.g. particle image velocimetry (PIV) patterns) and continuous passive scalar patterns (e.g. laser-sheet-induced fluorescence patterns in fluids). When discrete particle patterns are so coarse that an individual particle can be tracked, the local optic flow $\boldsymbol{u} = d\boldsymbol{x}/dt$ is the velocity of the particle in the image plane [20-21]. For dense discrete particle patterns, the local optic flow $\boldsymbol{u} = d\boldsymbol{x}/dt$ can be obtained using PIV method to seek the maximum correlation between two particle patterns obtained at two consecutive instants. However, for continuous passive scalar patterns, recovering the local optic flow $\boldsymbol{u} = d\boldsymbol{x}/dt$ is non-trivial since we have to consider the perspective projection of the transport equations of passive scalar through a specific imaging process. Generally speaking, the perspective projection of physical processes will lead to motion equations of image intensity. The optic flow $\boldsymbol{u} = d\boldsymbol{x}/dt$ is determined by solving the motion equation of image intensity for a specific physical process given the suitable boundary conditions and constraints. Detailed discussion on motion equations of image intensity will be given in Section 12.

6. The Correspondence Problem

In Sections 4 and 5, three unknown coordinates in the object space are reduced to two when the surface constraint is imposed. Thus, the correspondence between the constrained surface and the image plane is one-to-one. In order to determine three unknown coordinates from multiple views without any *a priori* constraint, however, we need to know the point correspondence between two or more images for the same physical point in the object space. This is the so-called point correspondence problem, one of the fundamental problems in 3D vision. Note that another correspondence problem is point correspondence in a time sequence of images. Here we focus on the

stereoscopic correspondence of images rather than the temporal correspondence.

Longuet-Higgins [22] gave a relation between the corresponding points in two images. Consider two cameras in which the unit vectors $(\boldsymbol{m}_{1(n)}, \boldsymbol{m}_{2(n)}, \boldsymbol{m}_{3(n)})$ constitute a local right-hand coordinate system whose origin is located at the perspective center $\boldsymbol{X}_{c(n)}$, where $n = 1,2$ is the index denoting the cameras 1 and 2. The three-dimensional coordinates $\boldsymbol{X}_{(n)} = (X^1_{(n)}, X^2_{(n)}, X^3_{(n)})^T$ in the coordinate frames $(\boldsymbol{m}_{1(n)}, \boldsymbol{m}_{2(n)}, \boldsymbol{m}_{3(n)})$ are related by a tensor-form of the translation and rotation transformations

$$X^{\alpha}_{(2)} = R_{\alpha\beta}(X^{\beta}_{(1)} - T^{\beta}_{r}), \tag{6.1}$$

where $\boldsymbol{R} = [R_{\alpha\beta}]$ and $\boldsymbol{T_r} = [T_r^{\beta}]$ are the rotation matrix and translation vector, respectively. If the two cameras have the same principal distance and pixel spacing ratio, $\boldsymbol{R}$ and $\boldsymbol{T_r}$ can be obtained by translating the origins $\boldsymbol{X}_{c(n)}$ and rotating the vectors $(\boldsymbol{m}_{1(n)}, \boldsymbol{m}_{2(n)}, \boldsymbol{m}_{3(n)})$ $(n = 1,2)$ to match the two coordinates frames. Here $\boldsymbol{R}$ and $\boldsymbol{T_r}$ are generally treated as the unknown matrix and vector.

A new matrix $\boldsymbol{Q}$ is given by

$$\boldsymbol{Q} = \boldsymbol{R}\,\boldsymbol{S} \quad \text{or} \quad S_{\alpha\beta} = R_{\alpha\mu}\, S_{\mu\beta}, \tag{6.2}$$

where $\boldsymbol{S}$ is the skew-symmetric matrix

$$\boldsymbol{S} = \begin{pmatrix} 0 & T_r^3 & -T_r^2 \\ -T_r^3 & 0 & T_r^1 \\ T_r^2 & -T_r^1 & 0 \end{pmatrix}. \tag{6.3}$$

Eq. (6.3) is written as a tensor notation

$$S_{\mu\beta} = \varepsilon_{\mu\beta\sigma} T_r^{\sigma}, \tag{6.4}$$

where the permutation index $\varepsilon_{\mu\beta\sigma} = 1, or\ -1, or\ 0$ if (μ,β,σ) is an even, or odd permutation of $(1,2,3)$, or otherwise. From Eqs. (6.1)-(6.4), we know

$$\begin{aligned} X^{\alpha}_{(2)}\, Q_{\alpha\beta}\, X^{\beta}_{(1)} &= R_{\alpha\kappa}(X^{\kappa}_{(1)} - T_r^{\kappa}) R_{\alpha\mu} \varepsilon_{\mu\beta\sigma}\, T_r^{\sigma} X^{\beta}_{(1)} \\ &= (X^{\mu}_{(1)} - T_r^{\mu}) \varepsilon_{\mu\beta\sigma}\, T_r^{\sigma} X^{\beta}_{(1)} = 0 \end{aligned}, \tag{6.5}$$

since $\boldsymbol{R}$ is orthogonal $(R_{\alpha\mu} R_{\mu\beta} = \delta_{\alpha\beta})$ and $\varepsilon_{\mu\beta\sigma}$ is anti-symmetric in every pair of its subscripts. Note that $\boldsymbol{X}_{(n)} = (X^1_{(n)}, X^2_{(n)}, X^3_{(n)})^T$ are the coordinates in the local frame $(\boldsymbol{m}_{1(n)}, \boldsymbol{m}_{2(n)}, \boldsymbol{m}_{3(n)})$ whose origin is located at the perspective center. Thus, the collinearity equations Eq. (2.2) can be re-written as a simpler form. In the local coordinate frames $(\boldsymbol{m}_{1(n)}, \boldsymbol{m}_{2(n)}, \boldsymbol{m}_{3(n)})$, without the lens distortion, the homogenous image coordinates $[x^{\alpha}_{h(n)}] = (x^1_{(n)}, x^2_{(n)}, -c)^T$ are related to the object space coordinates $X^{\alpha}_{(n)}$ by

$$x^{\alpha}_{h(n)} = -c\, X^{\alpha}_{(n)} / X^3_{(n)}. \quad (n = 1,2, \alpha = 1,2,3) \tag{6.6}$$

The image coordinates $x^{\alpha}_{(n)}$ are relative to the principal point in these local frames rather than the geometrical center of the image. Dividing Eq. (6.6) by $X^3_{(1)} X^3_{(2)} / c^2$ yields the Longuet-Higgins equation for the image point correspondence

$$x^{\alpha}_{h(2)}\, Q_{\alpha\beta}\, x^{\beta}_{h(1)} = 0. \tag{6.7}$$

Often, $\boldsymbol{Q} = [Q_{\alpha\beta}]$ is called the fundamental matrix that is related to the camera exterior orientation parameters. Given a number of the point correspondences between the two images (more than eight), the elements $Q_{\alpha\beta}$ can be determined by solving the following algebraic equations using a least-squares method

$$(x^{\alpha}_{h(2)}\, x^{\beta}_{h(1)})_i\, Q_{\alpha\beta} = 0. \quad (i = 1,2,\cdots) \tag{6.8}$$

Longuet-Higgins' original derivation of Eq. (6.7) is purely algebraic without giving a geometrical interpretation. In fact, the geometrical meaning of Eq. (6.7) is related to the epipolar lines in the images [2-3]. Given a point $(x^1_{(1)}, x^2_{(1)})$ in the image 1, its epipolar line in the image 2 is a projection of the line connecting the object space point and the image point through the optical center in the camera 1 onto the image 2. The epipolar line in the image 2 is described by

$$x^{\alpha}_{h(2)}\, p_{\alpha(1)} = 0, \tag{6.9}$$

where $p_{\alpha(1)} = Q_{\alpha\beta}\, x^{\beta}_{h(1)}$ are the coefficients of the epipolar line. Thus, the matrix $\boldsymbol{Q}$ maps the points in the image 1 to the epipolar lines in the image 2. In the same way, Eq. (6.7) also gives an epipolar line in the image 1 for a given point in the image 2. Hence, Eq. (6.7) serves as the epipolar constraint to reduce the number of unknowns in establishing the point correspondence. It is easily shown that when the lens distortion exists, the generalized epipolar constraint is

$$(x^{\alpha}_{h(2)} + \delta x^{\alpha}_{h(2)}) Q_{\alpha\beta} (x^{\beta}_{h(1)} + \delta x^{\beta}_{h(1)}) = 0. \tag{6.10}$$

The lens distortion terms are $[\delta x^{\alpha}_{h(n)}] = (\delta x^1_{(n)}, \delta x^2_{(n)}, 0)^T$. Since the lens distortion terms in Eqs. (2.4) and (2.5) are non-linear, an epipolar line is a curve rather than a straight line. More point correspondences are required to solve Eq. (6.10) since there are additional unknowns associated with the lens distortion.

The unknown fundamental matrix in the epipolar constraint is determined by using a number of point correspondences. Nevertheless, for two calibrated cameras, the image point correspondence can be directly established from the collinearity equations. The collinearity equations Eq. (2.9) for two cameras are written as

$$\begin{aligned} \boldsymbol{W}_{1(n)}{}^T (\boldsymbol{X} - \boldsymbol{X}_{c(n)}) = 0 \\ \boldsymbol{W}_{2(n)}{}^T (\boldsymbol{X} - \boldsymbol{X}_{c(n)}) = 0 \end{aligned}. \quad (n = 1,2) \tag{6.11}$$

Re-combination of Eq. (6.11) yields two sets of linear equations for $\boldsymbol{X}$

$$\boldsymbol{W}_{1com}\boldsymbol{X} = \boldsymbol{B}_{1com} \tag{6.12}$$

and

$$\boldsymbol{W}_{2com}\boldsymbol{X} = \boldsymbol{B}_{2com}\,, \tag{6.13}$$

where the composite matrices and vectors are

$$\boldsymbol{W}_{1com} = \begin{pmatrix} \boldsymbol{W}_{1(1)}^{\ T} \\ \boldsymbol{W}_{2(1)}^{\ T} \\ \boldsymbol{W}_{1(2)}^{\ T} \end{pmatrix},\ \boldsymbol{W}_{2com} = \begin{pmatrix} \boldsymbol{W}_{1(1)}^{\ T} \\ \boldsymbol{W}_{2(1)}^{\ T} \\ \boldsymbol{W}_{2(2)}^{\ T} \end{pmatrix},$$

$$\boldsymbol{B}_{1com} = \begin{pmatrix} \boldsymbol{W}_{1(1)}^{\ T}\boldsymbol{X}_{c(1)} \\ \boldsymbol{W}_{2(1)}^{\ T}\boldsymbol{X}_{c(1)} \\ \boldsymbol{W}_{1(2)}^{\ T}\boldsymbol{X}_{c(2)} \end{pmatrix},\ \boldsymbol{B}_{2com} = \begin{pmatrix} \boldsymbol{W}_{1(1)}^{\ T}\boldsymbol{X}_{c(1)} \\ \boldsymbol{W}_{2(1)}^{\ T}\boldsymbol{X}_{c(1)} \\ \boldsymbol{W}_{2(2)}^{\ T}\boldsymbol{X}_{c(2)} \end{pmatrix}. \tag{6.14}$$

Eliminating $\boldsymbol{X}$ from Eqs. (6.12) and (6.13), we have a relation between the image coordinates $(x^1_{(1)}, x^2_{(1)})$ in the image 1 and $(x^1_{(2)}, x^2_{(2)})$ in the image 2

$$\boldsymbol{G}(x^1_{(1)}, x^2_{(1)}; x^1_{(2)}, x^2_{(2)}) = \boldsymbol{W}_{1com}\,\boldsymbol{W}^{-1}_{2com}\boldsymbol{B}_{2com} - \boldsymbol{B}_{1com} = \boldsymbol{0}\,. \tag{6.15}$$

For a point $(x^1_{(1)}, x^2_{(1)})$ in the image 1, the corresponding epipolar line in the image 2 is given by

$$\| \boldsymbol{G}(x^1_{(1)}, x^2_{(1)}; x^1_{(2)}, x^2_{(2)}) \| = 0\,. \tag{6.16}$$

The Longuet-Higgins equation indicates that a point in the image 1 corresponds to the epipolar line on the image 2 and vice versa. Therefore, the point correspondence is not uniquely established between a pair of images since given an image point $(x^1_{(1)}, x^2_{(1)})$, there is only one equation for two unknowns $(x^1_{(2)}, x^2_{(2)})$. In order to establish the point correspondence among images, we need at least four cameras (or four images). For four cameras or images, the Longuet-Higgins equations are

$$x^{\alpha}_{h(i)}\, Q_{\alpha\beta(i-j)}\, x^{\beta}_{h(j)} = 0\,.\ (i = 1,2,3,4\,,\ j = 1,2,3,4) \tag{6.17}$$

If the fundamental matrices $Q_{\alpha\beta(i-j)}$ are determined by calibration, for a given point $(x^1_{(1)}, x^2_{(1)})$ in the image 1, we have a system of six algebraic equations for six unknowns $(x^1_{(1)}, x^2_{(1)}, x^1_{(2)}, x^2_{(2)}, x^1_{(3)}, x^2_{(3)})$

$$\begin{aligned} &x^{\alpha}_{h(1)}\, Q_{\alpha\beta(1-2)}\, x^{\beta}_{h(2)} = 0\,,\ x^{\alpha}_{h(1)}\, Q_{\alpha\beta(1-3)}\, x^{\beta}_{h(3)} = 0\,, \\ &x^{\alpha}_{h(2)}\, Q_{\alpha\beta(2-3)}\, x^{\beta}_{h(3)} = 0\,,\ x^{\alpha}_{h(1)}\, Q_{\alpha\beta(1-4)}\, x^{\beta}_{h(4)} = 0\,, \\ &x^{\alpha}_{h(2)}\, Q_{\alpha\beta(2-4)}\, x^{\beta}_{h(4)} = 0\,,\ x^{\alpha}_{h(3)}\, Q_{\alpha\beta(3-4)}\, x^{\beta}_{h(4)} = 0\,. \end{aligned} \tag{6.18}$$

When the four cameras are suitably positioned, Eq. (6.18) is not singular and the solution of Eq. (6.18) for $(x^1_{(1)}, x^2_{(1)}, x^1_{(2)}, x^2_{(2)}, x^1_{(3)}, x^2_{(3)})$ can be obtained using an iterative method. In general, there are multiple solutions since three equations in Eq. (6.18) are quadratic. The correct solution has to be selected based on additional criteria. More than four cameras can be used to increase the redundancy for least square estimation.

7. Composite Image Space and Object Space

Eq. (6.12) gives a non-linear relation between the object space coordinates and $\boldsymbol{X}$ and the composite image coordinates $\boldsymbol{x}_{com} = (x^1_{(1)}, x^2_{(1)}, x^1_{(2)})^T$. As shown in Fig. 7, the local coordinate frame $(\boldsymbol{m}_{1(1)}, \boldsymbol{m}_{2(1)}, \boldsymbol{m}_{3(1)})$ at the perspective center $\boldsymbol{X}_{c(1)}$ on the image 1 can serve as a frame for the composite image space in which $\boldsymbol{x}_{com} = (x^1_{(1)}, x^2_{(1)}, x^1_{(2)})^T$ are the coordinates along the unit vectors $(\boldsymbol{m}_{1(1)}, \boldsymbol{m}_{2(1)}, \boldsymbol{m}_{3(1)})$. Note that the coordinate $x^1_{(2)}$ of the corresponding point in the image 2 is artificially assigned to the coordinate value in the axis $\boldsymbol{m}_{3(1)}$ in the composite image space. Mapping between the composite image space and the object space is one-to-one. Differentiating Eq. (6.12), we have

$$\boldsymbol{W}_{1com}\, d\boldsymbol{X} + d\boldsymbol{W}_{1com}\,\boldsymbol{X} = d\boldsymbol{B}_{1com}\,. \tag{7.1}$$

Substitution of Eqs. (2.10), (6.12) and (6.14) into Eq. (7.1) yields a basic differential relation between the composite image space and object space (see Fig. 7)

$$d\boldsymbol{X} = \boldsymbol{H}(\boldsymbol{x}_{com})\, d\boldsymbol{x}_{com} \ \text{ or } \ dX^{\alpha} = H_{\alpha\beta}(\boldsymbol{x}_{com})\, dx^{\beta}_{com}\,, \tag{7.2}$$

where

$$\boldsymbol{H}(\boldsymbol{x}_{com}) = \boldsymbol{W}^{-1}_{1com} \begin{pmatrix} \boldsymbol{m}_{3(1)}^{\ T}(\boldsymbol{W}^{-1}_{1com}\boldsymbol{B}_{1com} - \boldsymbol{X}_{c(1)}) & 0 & 0 \\ 0 & \boldsymbol{m}_{3(1)}^{\ T}(\boldsymbol{W}^{-1}_{1com}\boldsymbol{B}_{1com} - \boldsymbol{X}_{c(1)}) & 0 \\ 0 & 0 & \boldsymbol{m}_{3(2)}^{\ T}(\boldsymbol{W}^{-1}_{1com}\boldsymbol{B}_{1com} - \boldsymbol{X}_{c(2)}) \end{pmatrix} \tag{7.3}$$

Consider a 3D curve in the object space. The arc length dS of the curve in the object space is expressed in the composite image coordinates, i.e.

$$dS^2 = dX^{\alpha} dX^{\alpha} = J_{\alpha\beta}\, dx^{\alpha}_{com} dx^{\beta}_{com}\,, \tag{7.4}$$

where $J_{\alpha\beta} = H_{\mu\alpha} H_{\mu\beta}$. Introducing the arc length $ds = (dx^{\alpha}_{com} dx^{\alpha}_{com})^{1/2}$ in the composite image space, we obtain a relation between dS and ds

$$dS = L(\boldsymbol{x}_{com})\, ds\,. \tag{7.5}$$

The length scale factor $L(\boldsymbol{x}_{com})$ is

$$L(\boldsymbol{x}_{com}) = (J_{\alpha\beta}\, t^{\alpha}_{com}\, t^{\beta}_{com})^{1/2}\,, \tag{7.6}$$

where $t^{\alpha}_{com} = dx^{\alpha}_{com} / ds$ is the unit tangent vector $\boldsymbol{t}_{com}$ of the corresponding curve in the composite image space. Using Eq. (7.5), we are able to express the unit tangent vector $\boldsymbol{T}$ of the curve in the object space in the composite image space coordinates and tangent vector, i.e.,

$$T^{\alpha} = dX^{\alpha}/dS = L^{-1} H_{\alpha\beta}\, t^{\beta}_{com}\,. \tag{7.7}$$

The principal normal vector $\boldsymbol{K}$ of the curve in the object space is

$$K^{\alpha} = dT^{\alpha}/dS = L^{-1}\left[\frac{\partial(H_{\alpha\beta}L^{-1})}{\partial x^{\sigma}_{com}} t^{\sigma}_{com} t^{\beta}_{com} + L^{-1} H_{\alpha\beta} k^{\beta}_{com}\right], \tag{7.8}$$

where $k^{\alpha}_{com} = dt^{\alpha}_{com}/ds = d^2 t^{\alpha}_{com}/ds^2$ is the principal normal vector of the corresponding curve in the composite image space. In the derivation of Eq. (7.8), the relation $d/ds = t^{\alpha}_{com}\partial/\partial x^{\alpha}_{com}$ is used. The curvature of the curve in the object space is

$$\kappa_{obj} = (K^{\alpha}K^{\alpha})^{1/2}. \tag{7.9}$$

Eqs. (7.8) and (7.9) indicate that the curvature is not an invariant under the perspective projection transformation, which depends on not only k^{α}_{com}, but also t^{α}_{com} and the camera parameters. The unit principal normal vector $\boldsymbol{N}$ is obtained by normalizing $\boldsymbol{K}$

$$\boldsymbol{N} = \kappa^{-1}_{obj}\boldsymbol{K} \text{ and } N^{\alpha} = \kappa^{-1}_{obj}K^{\alpha}. \tag{7.10}$$

The unit binormal vector $\boldsymbol{B}$ of the curve in the object space is

$$\boldsymbol{B} = \boldsymbol{T}\times\boldsymbol{N} \text{ or } B^{\alpha} = \varepsilon_{\alpha\beta\sigma}T^{\beta}N^{\sigma}. \tag{7.11}$$

Thus, the torsion of the curve in the object space is

$$\tau_{obj} = -N^{\alpha}dB^{\alpha}/dS = -\kappa^{-1}_{obj}K^{\alpha}L^{-1}\varepsilon_{\alpha\beta\sigma}(N^{\beta}N^{\sigma} + T^{\beta}t^{\mu}_{com}\partial N^{\sigma}/\partial x^{\mu}_{com}). \tag{7.12}$$

In this stage, the geometric structures of the 3D curve such as the tangent, curvature and torsion are expressed as a function of the composite image space coordinates. In general, they are not differential invariants under the perspective projection transformation. In many applications, however, these geometric quantities are very useful since they are directly related to the physical properties associated with the curve. The useful physical properties can be extracted from them. For example, the motion of an isolated vortex filament (a good model for a tornado) is mainly determined by the curvature and torsion of the filament [17].

From Eq. (7.2), we can relate the motion field $U_{\alpha}(\boldsymbol{X}) = dX^{\alpha}/dt$ in the object space with the motion field $u_{\alpha}(\boldsymbol{x_{com}}) = dx^{\alpha}_{com}/dt$ in the composite image space

$$U_{\alpha}(\boldsymbol{X}) = H_{\alpha\beta}(\boldsymbol{x_{com}})u_{\alpha}. \tag{7.13}$$

The motion field $U_{\alpha}(\boldsymbol{X})$ can be decomposed into two components

$$U_{\alpha}(\boldsymbol{X}) = dX^{\alpha}(S(t),t)/dt = \partial X^{\alpha}/\partial t + T^{\alpha}dS/dt. \tag{7.14}$$

The first term $\partial X^{\alpha}/\partial t$ is the apparent velocity and the second is the deformation velocity along the curve. Similarly, $u_{\alpha}(\boldsymbol{x_{com}})$ has two components

$$u_{\alpha}(\boldsymbol{x_{com}}) = dx^{\alpha}_{com}(s(t),t)/dt = \partial x^{\alpha}_{com}/\partial t + t^{\alpha}_{com}ds/dt. \tag{7.15}$$

If the point correspondence of the curve at two successive instants is not known, Eq. (7.13) cannot be directly utilized to calculate the motion field $U_{\alpha}(\boldsymbol{X})$ form image measurements. The deformation ds/dt in the composite image space cannot be determined from images without using any additional physical constraint. Thus, we have to look for a global method for recovering the motion field that is briefly discussed in Section 3.

8. Perspective Invariants of 3D Curve

Construction of perspective algebraic and differential invariants for a 3D curve is difficult because the perspective projection transformation is non-linear. However, it is possible to construct semi-differential invariants in a special case of stereo image pair [23]. The perspective invariants are useful since they can directly give certain geometric features of the curve from non-calibrated images. We use the perspective projection transformation for a pair of images

$$\boldsymbol{x_{h(i)}} = \lambda_{(i)}\boldsymbol{P_{h(i)}}\boldsymbol{X_h}, \quad (i = 1,2) \tag{8.1}$$

where $\boldsymbol{x_{h(i)}} = (x^1_{(i)}, x^2_{(i)}, 1)^T$ is the homogenous image coordinates in a pair of images ($i = 1,2$), $\boldsymbol{X_h} = (X^1, X^2, X^3, 1)^T$ is the homogenous coordinates in the object space, and $\boldsymbol{P_h} = [P_{h(i)\,nm}]$ ($n = 1,2,3$, $m = 1,2,3,4$) are a 3×4 matrix that only depends on the camera orientation parameters (see Section 2). In general, the scaling factors $\lambda_{(i)} = -c_{(i)}/\boldsymbol{m_{3(i)}}^T(\boldsymbol{X} - \boldsymbol{X_{c(i)}})$ for the two images are not the same, which are related to the camera parameters and the position of a point in the object space. Here we consider a special but useful case in which the scaling factors in two images are equal, i.e.,

$$\lambda_{(1)} = \lambda_{(2)} = \lambda. \tag{8.2}$$

The condition Eq. (8.2) implies

$$c_{(1)} = c_{(2)},\ \boldsymbol{m_{3(1)}} = \boldsymbol{m_{3(2)}},\ \boldsymbol{m_{3(1)}}^T(\boldsymbol{X_{c(2)}} - \boldsymbol{X_{c(1)}}) = \boldsymbol{0}. \tag{8.3}$$

Eq. (8.3) indicates that the two images have a relative shift on the same plane normal to the vector $\boldsymbol{m_{3(1)}} = \boldsymbol{m_{3(2)}}$. This means that two cameras are placed side by side and their optical axes are in parallel. This coplanar condition allows us to combine the collinearity equations Eq. (8.1) for the two images, which makes construction of perspective invariants possible.

A relationship between the composite image space and the object space for a 3D curve is written as in the homogeneous coordinates

$$\boldsymbol{x_{hcom}}(s(S)) = \lambda(S)\boldsymbol{P_{hcom}}\boldsymbol{X_h}, \tag{8.4}$$

where $\boldsymbol{x_{hcom}} = (x^1_{(1)}, x^2_{(1)}, x^1_{(2)}, 1)^T$ is the composite homogeneous coordinates in the image space, $\boldsymbol{X_h} = (X^1, X^2, X^3, 1)^T$ is the homogenous coordinates in the object space, and $\boldsymbol{P_{hcom}}$ is a composite matrix

$$\boldsymbol{P}_{hcom} = \begin{pmatrix} P_{h(1)11} & P_{h(1)12} & P_{h(1)13} & P_{h(1)14} \\ P_{h(1)21} & P_{h(1)22} & P_{h(1)23} & P_{h(1)24} \\ P_{h(2)11} & P_{h(2)12} & P_{h(2)13} & P_{h(2)14} \\ P_{h(1)31} & P_{h(1)32} & P_{h(1)33} & P_{h(1)34} \end{pmatrix}. \quad (8.5)$$

The arc lengths s and S of the curves in Eq. (8.4) are used as a parameter of the curve in the composite image space $(x^1_{(1)}, x^2_{(1)}, x^1_{(2)})$ and the object space (X^1, X^2, X^3), respectively. The function $s = s(S)$ is one-to-one.

Brill et al. [23] has constructed projective invariants by differentiating Eq. (8.4) repeatedly with respect with S, arranging the results in matrix equations for several points on the curve, evaluating the determinants of the matrix equations, and then eliminating all the factors related to the imaging parameters. At first, following the method developed by Brill et al. [23], we consider a number of the basic geometric structures. The curvatures in the composite image space and the object space are [18]

$$\kappa_{im} = |\ddot{\boldsymbol{x}}_{com}| = |\dot{\boldsymbol{x}}_{com} \times \ddot{\boldsymbol{x}}_{com}| \text{ and } \kappa_{obj} = |\ddot{\boldsymbol{X}}| = |\dot{\boldsymbol{X}} \times \ddot{\boldsymbol{X}}|, \quad (8.6)$$

where $\dot{\boldsymbol{x}}_{com} = d\boldsymbol{x}_{com}/ds$, $\ddot{\boldsymbol{x}}_{com} = d^2\boldsymbol{x}_{com}/ds^2$, $\dot{\boldsymbol{X}} = d\boldsymbol{X}/dS$, and $\ddot{\boldsymbol{X}} = d^2\boldsymbol{X}/dS^2$ are the derivatives with respect to the arc length. The torsions in the composite image space and the object space are, respectively,

$$\begin{aligned} \tau_{im} &= |\dot{\boldsymbol{x}}_{com}\ \ddot{\boldsymbol{x}}_{com}\ \dddot{\boldsymbol{x}}_{com}| / |\ddot{\boldsymbol{x}}_{com}|^2 \\ &= -|\dot{\boldsymbol{x}}_{hcom}\ \ddot{\boldsymbol{x}}_{hcom}\ \dddot{\boldsymbol{x}}_{hcom}| / |\ddot{\boldsymbol{x}}_{com}|^2 \end{aligned}, \quad (8.7)$$

and

$$\tau_{obj} = |\dot{\boldsymbol{X}}\ \ddot{\boldsymbol{X}}\ \dddot{\boldsymbol{X}}| / |\ddot{\boldsymbol{X}}|^2 = -|\dot{\boldsymbol{X}}_{\boldsymbol{h}}\ \ddot{\boldsymbol{X}}_{\boldsymbol{h}}\ \dddot{\boldsymbol{X}}_{\boldsymbol{h}}| / |\ddot{\boldsymbol{X}}|^2. \quad (8.8)$$

Eqs. (8.7) and (8.8) are expressed in the homogeneous coordinates $\boldsymbol{x}_{hcom} = (x^1_{(1)}, x^2_{(1)}, x^1_{(2)}, 1)^T$ and $\boldsymbol{X}_{\boldsymbol{h}} = (X^1, X^2, X^3, 1)^T$ to facilitate the use of Eq. (8.4). In the object space, the unit tangent vector is $\boldsymbol{T} = \dot{\boldsymbol{X}}$, the unit principal normal vector is $\boldsymbol{N} = \ddot{\boldsymbol{X}}/\kappa_{obj}$, and the unit binormal vector is $\boldsymbol{B} = \boldsymbol{T} \times \boldsymbol{N} = \dot{\boldsymbol{X}} \times \ddot{\boldsymbol{X}}/\kappa_{obj}$. We define the distance D_{ij} from a point $\boldsymbol{X}_i$ to the osculating plane to the curve at another point $\boldsymbol{X}_j$

$$\begin{aligned} D_{ij} &= (\boldsymbol{X}_j - \boldsymbol{X}_i) \bullet \boldsymbol{B}_j = |(\boldsymbol{X}_j - \boldsymbol{X}_i)\ \dot{\boldsymbol{X}}_j\ \ddot{\boldsymbol{X}}_j| / \kappa_{obj,j} \\ &= |\boldsymbol{X}_{h,j}\ \dot{\boldsymbol{X}}_{h,j}\ \ddot{\boldsymbol{X}}_{h,j}\ \boldsymbol{X}_{h,i}| / \kappa_{obj,j} \end{aligned}, \quad (8.9)$$

where the subscripts 'i' and 'j' denote the quantities associated with the points $\boldsymbol{X}_i$ and $\boldsymbol{X}_j$. The geometrical meaning of D_{ij} is illustrated in Fig. 8. Similarly, in the composite image space, the distance d_{ij} from a point $\boldsymbol{x}_{com,i}$ to the osculating plane to the curve at the point $\boldsymbol{x}_{com,j}$

$$\begin{aligned} d_{ij} &= |(\boldsymbol{x}_{hcom,j} - \boldsymbol{x}_{hcom,i})\ \dot{\boldsymbol{x}}_{hcom,j}\ \ddot{\boldsymbol{x}}_{hcom,j}| / \kappa_{im,j} \\ &= |\boldsymbol{x}_{hcom,j}\ \dot{\boldsymbol{x}}_{hcom,j}\ \ddot{\boldsymbol{x}}_{hcom,j}\ \boldsymbol{x}_{hcom,i}| / \kappa_{im,j} \end{aligned}. \quad (8.10)$$

In addition, we introduce the following geometric quantities

$$\begin{aligned} i(1,1',2,3) &= |\boldsymbol{x}_{hcom,1}\ \dot{\boldsymbol{x}}_{hcom,1}\ \boldsymbol{x}_{hcom,2}\ \boldsymbol{x}_{hcom,3}|, \\ i(1,2,2',3) &= |\boldsymbol{x}_{hcom,1}\ \boldsymbol{x}_{hcom,2}\ \dot{\boldsymbol{x}}_{hcom,2}\ \boldsymbol{x}_{hcom,3}|, \\ I(1,1',2,3) &= |\boldsymbol{X}_{h,1}\ \dot{\boldsymbol{X}}_{h,1}\ \boldsymbol{X}_{h,2}\ \boldsymbol{X}_{h,3}|, \\ I(1,2,2',3) &= |\boldsymbol{X}_{h,1}\ \boldsymbol{X}_{h,2}\ \dot{\boldsymbol{X}}_{h,2}\ \boldsymbol{X}_{h,3}|. \end{aligned} \quad (8.11)$$

Differentiating Eq. (8.4) with respect to S, we obtain

$$\begin{aligned} \dot{\boldsymbol{x}}_{hcom,i} &= \dot{s}^{-1} \boldsymbol{P}_{hcom} (\boldsymbol{X}_{h,i}\ \dot{\boldsymbol{X}}_{h,i}) \begin{pmatrix} \dot{\lambda}_i \\ \lambda_i \end{pmatrix}, \\ \ddot{\boldsymbol{x}}_{hcom,i} &= \dot{s}^{-2} \boldsymbol{P}_{hcom} (\boldsymbol{X}_{h,i}\ \dot{\boldsymbol{X}}_{h,i}\ \ddot{\boldsymbol{X}}_{h,i}) \begin{pmatrix} \xi_{1i} \\ \xi_{2i} \\ \lambda_i \end{pmatrix}, \\ \dddot{\boldsymbol{x}}_{hcom,i} &= \dot{s}^{-3} \boldsymbol{P}_{hcom} (\boldsymbol{X}_{h,i}\ \dot{\boldsymbol{X}}_{h,i}\ \ddot{\boldsymbol{X}}_{h,i}\ \dddot{\boldsymbol{X}}_{h,i}) \begin{pmatrix} \dot{\xi}_{1i} - 2\ddot{s}\xi_{1i} \\ \xi_{1i} + \dot{\xi}_{2i} - 2\ddot{s}\xi_{2i} \\ \xi_{2i} + \lambda_i + 2\ddot{s}\lambda_i \\ \lambda_i \end{pmatrix} \end{aligned} \quad (8.12)$$

where $\xi_{1i} = \ddot{\lambda}_i - \dot{\lambda}_i \ddot{s} \dot{s}^{-1}$, $\xi_{2i} = 2\dot{\lambda}_i - \lambda_i \ddot{s} \dot{s}^{-1}$, and $\dot{s} = ds(S)/dS$. From Eqs. (8.6)-(8.12), we have the following determinantal relations

$$\kappa^2_{im,i}\ \tau_{im,i} = \lambda_i^4 \dot{s}^{-6} |\boldsymbol{P}_{hcom}| \kappa^2_{obj,i}\ \tau_{obj,i}, \quad (8.13)$$

$$\kappa_{im,j}\ d_{ij} = \lambda_i\ \lambda_j^3\ \dot{s}^{-3} |\boldsymbol{P}_{hcom}| \kappa_{obj,j}\ D_{ij}, \quad (8.14)$$

$$i(1,1',2,3) = \lambda_1^2\ \lambda_2\ \lambda_3\ \dot{s}^{-3} |\boldsymbol{P}_{hcom}| I(1,1',2,3), \quad (8.15)$$

$$i(1,2,2',3) = \lambda_2^2\ \lambda_1\ \lambda_3\ \dot{s}^{-3} |\boldsymbol{P}_{hcom}| I(1,2,2',3). \quad (8.16)$$

The subscripts 'i' and 'j' denote the quantities associated with the points $\boldsymbol{X}_i$ and $\boldsymbol{X}_j$ in the object space and the corresponding points $\boldsymbol{x}_{com,i}$ and $\boldsymbol{x}_{com,j}$ in the composite image space. Re-arrangement of Eqs. (8.13)-(8.16) to eliminate λ_1, λ_2, $\dot{s}$, and $|\boldsymbol{P}_{hcom}|$ yields several semi-differential perspective invariants.

(I) An invariant related to the torsions and the distances D_{ij} and d_{ij} is

$$\frac{\tau_{im,1}\ d_{12}^2}{\tau_{im,2}\ d_{21}^2} = \frac{\tau_{obj,1}\ D_{12}^2}{\tau_{obj,2}\ D_{21}^2}. \quad (8.17)$$

For $\tau_{obj,1} = 0$, $\tau_{obj,2} \neq 0$, $D_{12} \neq 0$, and $D_{21} \neq 0$, then $\tau_{im,1} = 0$. The zero-torsion point in the object space corresponds to the zero-torsion point in the composite image space. The condition $D_{12} \neq 0$, and $D_{21} \neq 0$

implies that the points $\boldsymbol{X}_1$ and $\boldsymbol{X}_2$ are not on the same osculating plane.

(II) An invariant related to the curvatures, the distances D_{ij} and d_{ij}, and the quantities $i(1,1',2,3)$, $i(1,2,2',3)$, $I(1,1',2,3)$ and $I(1,2,2',3)$ is

$$\frac{\kappa_{im,2}\, d_{12}\, i^2(1,1',2,3)}{\kappa_{im,1}\, d_{21}\, i^2(1,2,2',3)} = \frac{\kappa_{obj,2}\, D_{12}\, I^2(1,1',2,3)}{\kappa_{obj,1}\, D_{21}\, I^2(1,2,2',3)}. \quad (8.18)$$

For $\kappa_{obj,2} = 0$, $\kappa_{obj,1} \neq 0$, $D_{12} \neq 0$, and $D_{21} \neq 0$, then $\kappa_{im,2} = 0$. This means that the zero-curvature point in the object space corresponds to the zero-curvature point in the composite image space.

(III) An invariant related to the distances D_{ij} and d_{ij} is

$$\frac{d_{21}\, d_{43}}{d_{41}\, d_{23}} = \frac{D_{21}\, D_{43}}{D_{41}\, D_{23}}. \quad (8.19)$$

This result is analogous to the cross-ratio of the distances on a line, a classical perspective invariant in perspective geometry [2, 24].

9. Modeling of Imaging System

Modeling of an imaging system is necessary for radiometric measurements. Figure 9 shows a radiation source at an infinitesimal area element dA_s on the optical axis, having a distance R_1 from the optical center of the imaging system like a CCD camera [25]. The radiant energy (units: joule) from the area element integrated over a solid angle seen from dA_s to a lens is

$$dQ = dA_s\, dt \int L(\theta,\phi)\cos\theta\, d\omega, \quad (9.1)$$

where $L(\theta,\phi)$ is the radiance (units: watt-m^{-2}-sr^{-1}) of the radiative source at dA_s, $d\omega = \sin\theta\, d\theta\, d\phi$ is the infinitesimal element of solid angle, θ is the polar angle (measured from the surface normal), ϕ is the azimuthal angle (measured between an arbitrary axis on the surface and the element of solid angle on the surface), and dt is a time interval. The number of photons collected by the lens is

$$\begin{aligned} dn_{lens} &= (\hbar\nu)^{-1} T_{atm}\, dQ \\ &= (\hbar\nu)^{-1}\, dA_s\, dt\, T_{atm} \int L(\theta,\phi)\cos\theta\, d\omega \end{aligned}. \quad (9.2)$$

where $\hbar\nu$ is the energy of a single photon and T_{atm} is the transmittance of atmosphere air. Define θ_A as the angle between the optical axis and the line connecting dA_s and the edge of the aperture. When θ_A is small, $(\sin\theta_A)^2 \approx A_0 / R_1^2$ is approximately the solid angle in which the radiative energy from dA_s is collected by the imaging system, where A_0 is the imaging system aperture entrance area. Thus, Eq. (9.2) becomes

$$dn_{lens} = L_p\, dA_s\, dt\, T_{atm}\, (A_0 / R_1^2), \quad (9.3)$$

where L_p is the average photon radiance over the collecting solid angle $A_0 / R_1^2 \approx (\sin\theta_A)^2$

$$L_p = (\hbar\nu)^{-1} (\sin\theta_A)^{-2} \int L(\theta,\phi)\cos\theta\, d\omega. \quad (9.4)$$

Consequently, the number of photons reaching the image plane is

$$dn_{im} = L_p\, dA_s\, dt\, (A_0 / R_1^2) T_{atm} T_{opt}, \quad (9.5)$$

where T_{opt} is the transmittance of the optical system. The number of photons incident the detector element is simply proportional to a ratio between the detector element area A_D and the image area dA_I corresponding to dA_s

$$dn_{det} = dn_{im}\, A_D / dA_I. \quad (9.6)$$

Under the approximation of small angle $\theta_A << 1$, dA_I is related to dA_s by

$$dA_s / R_1^2 = dA_I / R_2^2, \quad (9.7)$$

where R_2 is the distance of the image plane from the optical center. Substituting Eqs. (9.5) and (9.7) to Eq. (9.6) and using the relations $A_0 = \pi D^2 / 4$ and $1/R_2 + 1/R_1 = 1/fl$, we have

$$dn_{det} = \frac{\pi}{4} \frac{L_p\, A_D\, dt\, T_{atm} T_{opt}}{F^2 (1 + M_{opt})^2}, \quad (9.8)$$

where $F = fl / D$ is the F-number and $M_{opt} = R_2 / R_1$ is the optical magnification, D is the diameter of the aperture, and fl is the focal length. Thus, the total number of photons collected over an integration time t_{INT} is

$$n_{det} = \frac{\pi}{4} \frac{L_p\, A_D\, t_{INT}\, T_{atm} T_{opt}}{F^2 (1 + M_{opt})^2}. \quad (9.10)$$

Since some of the variables in Eq. (9.10) depend on the frequency ν of light, the number of photoelectrons generated in the solid-state detector over a frequency band $[\nu_1, \nu_2]$ is

$$n_{pe} = \int_{\nu_1}^{\nu_2} R_g(\nu) \frac{\pi}{4} \frac{L_p(\nu)\, A_D\, t_{INT}\, T_{atm}(\nu) T_{opt}(\nu)}{F^2 (1 + M_{opt})^2} d\nu, \quad (9.11)$$

where $R_g(\nu)$ is the detector's quantum efficiency (units: electrons/phonon). We separate the photon radiance L_p into the radiance magnitude $\overline{L_p}$ independent of ν and a shape function of the frequency spectrum $f_{sp}(\nu)$, i.e.,

$$L_p = \overline{L_p}\, f_{sp}(\nu). \quad (9.12)$$

Therefore, Eq. (9.11) becomes

$$n_{pe} = p_{cam}\,\overline{L_p}\,, \tag{9.13}$$

where p_{cam} is a parameter describing the camera performance

$$p_{cam} = \int_{\nu_1}^{\nu_2} R_g(\nu)\frac{\pi}{4}\frac{f_{sp}(\nu)A_D\,t_{INT}\,T_{atm}(\nu)T_{opt}(\nu)}{F^2(1+M_{opt})^2}d\nu\,. \tag{9.14}$$

After the camera is radiometrcally calibrated, the image intensity (gray level) is proportional to n_{pe}, i.e.,

$$I(\boldsymbol{x}) = c_{Im}\,n_{pe}\,. \tag{9.15}$$

The proportional constant c_{Im} is determined by calibration. The above analysis is made based on the assumption that the radiation source is on the optical line. In general, we have to take the off-axis effect into account [26-27]. Hence, a generalized form of Eq. (9.15) is

$$I(\boldsymbol{x}) = c_{Im}\,p_{cam}\,\overline{L_p}\cos^4\theta_p\,, \tag{9.16}$$

where θ_p is the angle between the optical axis and light ray through the optical center. When the lens distortion is negligible, the angle θ_p can be expressed as a function of the image coordinates $\boldsymbol{x}$, the principal point location $\boldsymbol{x_p}$ and the principal distance *c*, i.e.,

$$\theta_p = arctan(|\,\boldsymbol{x}-\boldsymbol{x_p}\,|/c)\,. \tag{9.17}$$

Grouping the terms in Eq. (9.16) that are only dependent of the image coordinates to the left-hand side, we get

$$I(\boldsymbol{x})\,O_x(|\,\boldsymbol{x}-\boldsymbol{x_p}\,|) = c_{Im}\,p_{cam}\,\overline{L_p}(\boldsymbol{X})\,, \tag{9.18}$$

where the function describing the off-axis effect can be approximated by

$$O_x(|\,\boldsymbol{x}-\boldsymbol{x_p}\,|) = \cos^{-4}\theta_p \approx 1+2\,|\,\boldsymbol{x}-\boldsymbol{x_p}\,|^2/c^2\,. \tag{9.19}$$

Assuming that the off-axis effect is corrected on the image plane, without loss of generality, we simply rewrite Eq. (9.18) as

$$I(\boldsymbol{x}) = c_{Im}\,p_{cam}\,\overline{L_p}(\boldsymbol{X})\,. \tag{9.20}$$

In order to simplify the notations, we use replacements $c_{sys} \to c_{Im}\,p_{cam}$ and $L(\boldsymbol{X}) \to \overline{L_p}(\boldsymbol{X})$. Therefore, without loss of generality, Eq. (9.20) becomes

$$I(\boldsymbol{x}) = c_{sys}\,L(\boldsymbol{X})\,, \tag{9.21}$$

where c_{sys} is a proportional constant related to the imaging system and $L(\boldsymbol{X})$ should be understood as the spectrally averaged radiance.

10. Typical Radiation Processes

Surface Reflection

Quantitative image-based measurements require the knowledge of the physical properties of radiation-matter interaction of the objects of interest. One of the important interactions is reflection on a surface. As shown in Fig. 10, the incident radiance is generally a function of the incident direction (θ_i,ϕ_i), i.e.,

$$L_i = L_i(\theta_i,\phi_i)\,. \tag{10.1}$$

The reflection radiance $L_r(\theta_i,\phi_i;\theta_r,\phi_r)$ is quantitatively characterized by the bidirectional reflectance distribution function (BRDF) [28]

$$f_r(\theta_i,\phi_i;\theta_r,\phi_r) = dL_r(\theta_i,\phi_i;\theta_r,\phi_r)/dE_i(\theta_i,\phi_i)\,. \tag{10.2}$$

where the infinitesimal incident irradiance $dE_i(\theta_i,\phi_i)$ over a solid angle element $d\omega_i$ is

$$dE_i(\theta_i,\phi_i) = L_i(\theta_i,\phi_i)\cos\theta_i\,d\omega_i\,. \tag{10.3}$$

The BRDF has a unit of steradian^{-1}. The BRDF depends on the surface roughness distribution. Foe a perfectly diffuse surface or a Lambertian surface where the reflection radiance is isotropic, i.e., $L_r = const.$, the BRDF is $f_r = 1/\pi$. In this case, the reflection radiance is

$$L_r = (1/\pi)\int_{\omega_i} L_i(\theta_i,\phi_i)\cos\theta_i\,d\omega_i\,. \tag{10.4}$$

Furthermore, when the incident source of the irradiance E_0 is collimated at a fixed incident direction (θ_0,ϕ_0), the incident radiance is described by the Dirac-delta function

$$L_i(\theta_i,\phi_i) = E_0\,\delta(\theta_i-\theta_0)\delta(\phi_i-\phi_0)/\sin\theta_0\,. \tag{10.5}$$

Thus, Eq. (10.4) becomes the Lambert's cosine law

$$L_r = (1/\pi)E_0\cos\theta_0\,. \tag{10.6}$$

For a general surface, the BRDF can be derived based on either the wave equation for electromagnetic waves or geometrical optics. Using the method of Helmholtz-Kirchhoff integral, Beckmann and Spizzichino [29] have derived an expression for the mean power of electromagnetic wave scattered from a rough surface. Similar integral approaches were used by Icart & Arques [30] and Wang [31]. Icart and Arques [30] derived an expression of the BRDF for multilayer materials, which was composed of specular, directional-diffuse (spread reflection), and uniform diffuse (Lambertian) components. From a viewpoint of geometrical optics, Torrance and Sparrow [32] gave a simpler expression for the BRDF. Beckmann-Spizzichino's model and Torrance-Sparrow's model were discussed by Nayar et al. [33] from a viewpoint of computer vision application. A bibliographical review on the BRDF was given by Asmail [34]. Scattering of electromagnetic waves from randomly rough surfaces is still an active research area covering a variety of theoretical and experimental studies [35].

From a viewpoint of application, the empirical expressions for the scattered radiance from a rough surface are very useful due to their simplicity [36]. An empirical model for a single light source is

$$\begin{aligned} L_r(\boldsymbol{X}) &= \rho_a\,E_a(\boldsymbol{X}) + \rho_d\,E_{ls}(\boldsymbol{X})(\boldsymbol{N}^T\boldsymbol{L_s}) \\ &\quad + \rho_s\,E_{ls}(\boldsymbol{X})\,p(\boldsymbol{R}^T\boldsymbol{V}) \end{aligned}, \tag{10.7}$$

where the first, second and third terms are, respectively, the contributions from the ambient reflection, diffuse reflection, and specular reflection. In Eq. (10.7), ρ_a, ρ_d,

and ρ_s, are the empirical reflection coefficients for the ambient reflection, diffuse reflection, and specular reflection. As shown in Fig. 11, the vectors $\boldsymbol{N}$, $\boldsymbol{L}_s$, $\boldsymbol{R}$, and $\boldsymbol{V}$ are, respectively, the unit normal vector of a surface, the unit vector directing the light source from the surface, the unit main directional vector of the specular reflection, and the unit viewing vector. $E_a(\boldsymbol{X})$ and $E_{ls}(\boldsymbol{X})$ are the irradiances for the ambient environment and light sources, respectively. The function $p(\boldsymbol{R}^T\boldsymbol{V})$ is the directional distribution of the specular reflection, describing the spreading of scattered light. Phong [37] gave a power function $p(\boldsymbol{R}^T\boldsymbol{V}) = (\boldsymbol{R}^T\boldsymbol{V})^n$. In general, the main directional vector of the specular reflection, $\boldsymbol{R}$, is a function of the incident direction of light $-\boldsymbol{L}_s$. Although there are theories for predicting $\boldsymbol{R}$ [32], it is not known for a general surface. The unknowns in Eq. (10.7), including $\boldsymbol{R}$, the reflection coefficients and the parameters in $p(\boldsymbol{R}^T\boldsymbol{V})$, have to be determined by calibration. For multiple light sources, Eq. (10.7) includes superposition of the contributions from these light sources.

Radiative Energy Transfer in Media

When light travels in a medium, the radiance is affected by absorption, emission and scattering. The radiative energy obeys overall conservation of energy. The equation of radiative energy transfer can be derived based on a balance among absorption, emission and scattering, i.e.,

$$\frac{dL_\eta}{ds} = \boldsymbol{s}\bullet\nabla L_\eta = S_\eta - \beta_\eta L_\eta + \frac{\sigma_{s\eta}}{4\pi}\int_{4\pi} L_\eta(\boldsymbol{s}_i)\Phi_\eta(\boldsymbol{s}_i,\boldsymbol{s})d\omega_i \tag{10.8}$$

where $\boldsymbol{s}$ is the path vector, β_η is the extinction coefficient, $\sigma_{s\eta}$ is the scattering coefficient, $\Phi_\eta(\boldsymbol{s}_i,\boldsymbol{s})$ is the scattering phase function, S_η is a radiation source term, and the subscript η denotes the frequency range. This transport equation has been used in radiative heat transfer [38] and radiative hydrodynamics [39]. Note that the terminology of the radiatve intensity (unit: watts/area/solid angle) used in literature of radiative heat transfer is just the radiance in radiometry. The solution techniques and the suitable boundary conditions have been discussed by Modest [38].

Luminescence

Luminescence is an emission from molecules after they are excited by an excitation light with a suitable wavelength. Luminescent dyes, widely used as probe molecules in biological and medical applications [40], have been utilized for flow visualization and measurements. For example, based on oxygen quenching of luminescence, luminescent molecules immobilized in a polymer layer have been used for surface pressure and temperature measurements in aerodynamic testing. These new sensors are called as pressure- and temperature-sensitive paints (TSP and PSP). After luminescent molecules in PSP absorb the energy from the excitation light with a wavelength λ_1, they emit luminescence with a longer wavelength λ_2 due to the Stokes shift. Liu et al. [41] have analyzed luminescent radiation from a PSP layer and obtained the spectral luminescent radiance (L_{λ_2})

$$L_{\lambda_2} = h\,\Phi(P,T)\,q_0\;Es_{\lambda_2}(\lambda_2)K_1(\beta_{\lambda_1}/\mu)M(\mu), \tag{10.9}$$

where $\Phi(P,T)$ is the luminescent quantum yield that depends on pressure (P) and temperature (T), $Es_{\lambda_2}(\lambda_2)$ is the luminescent emission spectrum, h is the layer thickness, q_0 is the incident light flux, $\mu = \cos\theta$ is the cosine of the polar angle θ, and the extinction coefficient $\beta_{\lambda_1} = \varepsilon_{\lambda_1} c$ is a product of the molar absorptivity ε_{λ_1} and luminescent molecule concentration c. The coefficient M represents the effects of reflection and scattering of the luminescent light at the wall. The term K_1 represents the combined effect of the optical filter, excitation light scattering, and direction of the incident excitation light. The luminescent irradiance E_{λ_2} over a collecting solid angle Ω is

$$\begin{aligned} E_{\lambda_2} &= \int_\Omega L_{\lambda_2}\cos\theta\, d\Omega \\ &= \beta_{\lambda_1} h\,\Phi(P,T)\,q_0\;Es_{\lambda_2}(\lambda_2)\;K_1 < M > \Omega \end{aligned}, \tag{10.10}$$

where $< M >$ is the spectrally averaged quantity of M. Even though Liu's analysis was focused on a thin PSP layer, calculation of luminescent radiance is generally valid for a luminescent volume where surface reflection is absent. The spectral luminescent radiance integrated over a volume V is expressed as

$$L_{\lambda_2} = Es_{\lambda_2}(\lambda_2)K_1\,\mu^{-1}\int_V \Phi(\boldsymbol{X})q_0(\boldsymbol{X})\;\beta_{\lambda_1}(\boldsymbol{X})d\boldsymbol{X}\,. \tag{10.10}$$

A similar analysis for the luminescent flux was given by Gaigalas et al. [42].

11. Reflection and Shape Recovery

Reflection on a solid surface depends on the geometric properties of the surface. In principle, shape of the surface can be recovered from surface reflectance under certain conditions. Computer vision scientists have studied the so-called shape-from-shading problem for decades [43-44]. Here we give a general consideration that is particularly useful for more complex engineering structures. Figure 11 shows a surface element with the unit normal vector $\boldsymbol{N}$. The incident polar angle θ_i is the angle between the unit normal vector $\boldsymbol{N}$ and the unit vector $\boldsymbol{L}_s$ directing the light source from the surface. The reflecting polar angle

θ_r is the angle between the unit normal vector $\boldsymbol{N}$ and the unit reflecting vector $\boldsymbol{R}$. The azimuthal angle ϕ_r is the angle between the projections of the vectors $\boldsymbol{L}_s$ and $\boldsymbol{R}$ on the surface. Assuming that the reflecting vector $\boldsymbol{R}$ is on the plane spanned by $\boldsymbol{L}_s$ and $\boldsymbol{N}$, we have

$$\boldsymbol{R} = a_N \boldsymbol{N} + a_L \boldsymbol{L}_s . \tag{11.1}$$

The coefficients a_N and a_L are determined by solving the following equations

$$\cos\theta_r = \boldsymbol{N} \bullet \boldsymbol{R} = a_N + a_L \boldsymbol{N} \bullet \boldsymbol{L}_s ,$$
$$\boldsymbol{R} \bullet \boldsymbol{R} = a_N^2 + 2 a_N a_L \boldsymbol{N} \bullet \boldsymbol{L}_s + a_L^2 = 1 . \tag{11.2}$$

Eliminating a_N from Eq. (11.2) yields

$$(1+\cos^2\theta_i) a_L^2 - 2\cos^2\theta_i \, a_L + \cos^2\theta_r - 1 = 0 . \tag{11.3}$$

There are two solutions for a_L

$$a_L = \frac{\cos^2\theta_i \pm \sqrt{(1+\cos^2\theta_i)(\cos^2\theta_i - \cos^2\theta_r)+1}}{1+\cos^2\theta_i} . \tag{11.4}$$

The reflecting polar angle θ_r is not necessarily equal to the incident angle θ_i especially at large incident angles due to the off-specular reflection phenomenon on a rough surface [32]. In general, $\theta_r \geq \theta_i$ insures that there is no imaginary solution for a_L, which is also supported by experiment data. The condition $\theta_r \geq \theta_i$ indicates $a_L \leq 0$. Thus, the appropriate solution for a_N and a_L are

$$a_L = \frac{\cos^2\theta_i - \sqrt{(1+\cos^2\theta_i)(\cos^2\theta_i - \cos^2\theta_r)+1}}{1+\cos^2\theta_i} ,$$
$$a_N = \cos\theta_r - a_L \cos\theta_i . \tag{11.5}$$

The reflecting polar angle θ_r can be expressed as a function of θ_i based on theories and experimental results. In a special, but very useful case $\theta_r = \theta_i$, Eq. (11.5) becomes

$$a_L = \frac{\cos^2\theta_i - 1}{1+\cos^2\theta_i} = \frac{(\boldsymbol{N} \bullet \boldsymbol{L}_s)^2 - 1}{1+(\boldsymbol{N} \bullet \boldsymbol{L}_s)^2} ,$$
$$a_N = \frac{2\cos\theta_i}{1+\cos^2\theta_i} = \frac{2\boldsymbol{N} \bullet \boldsymbol{L}_s}{1+(\boldsymbol{N} \bullet \boldsymbol{L}_s)^2} . \tag{11.6}$$

Consider a surface $X^3 = F(X^1, X^2)$ illuminated by a single light source. The relation between the image intensity and reflection radiance from the surface is

$$I(\boldsymbol{x}) = c_{sys} \rho_a \, E_a(\boldsymbol{X}) + c_{sys} E_{ls}(\boldsymbol{X}) [\rho_d \, \boldsymbol{N} \bullet \boldsymbol{L}_s + \rho_s \, p(\boldsymbol{R} \bullet \boldsymbol{V})] . \tag{11.7}$$

The relation between the image coordinates $\boldsymbol{x}$ and the object-space coordinates $\boldsymbol{X}$ is given by the collinearity equations Eq. (2.2). The unit normal vector $\boldsymbol{N}$ is

$$\boldsymbol{N} = (F_{X^1}, F_{X^2}, -1)^T / \sqrt{F_{X^1}^2 + F_{X^2}^2 + 1} , \tag{11.8}$$

where $F_{X^1} = \partial F / \partial X^1$ and $F_{X^2} = \partial F / \partial X^2$. The unit vector $\boldsymbol{L}_s$ directing the light source $\boldsymbol{X}_c$ from the surface is

$$\boldsymbol{L}_s = (\boldsymbol{X}_s - \boldsymbol{X}) / |\boldsymbol{X}_s - \boldsymbol{X}| . \tag{11.9}$$

When the camera is sufficiently away from the object, the unit viewing vector $\boldsymbol{V}$ directing from surface to the camera is approximately

$$\boldsymbol{V} = -\boldsymbol{m}_3 , \tag{11.10}$$

which is known for a photogrammetrically calibrated camera. The reflecting vector $\boldsymbol{R}$ is given by Eqs. (11.1), (11.5) and (11.6). Clearly, given an image intensity field $I(\boldsymbol{x})$, Eq. (11.7) is a complicated non-linear first-order partial differential equation for the surface $X^3 = F(X^1, X^2)$. Thus, a numerical solution to Eq. (11.7) has to be sought with suitable boundary conditions and constraints.

When the light source is away enough from the object relative to the size of the object, the incident irradiance $E_{ls}(\boldsymbol{X})$ and ambient irradiance $E_a(\boldsymbol{X})$ can be considered to be homogenous on the surface of the object, that is, $E_{ls}(\boldsymbol{X}) = const.$ and $E_a(\boldsymbol{X}) = const.$. In this case, the vector $\boldsymbol{L}_s$ is also approximately homogenous and it becomes a constant vector. Thus, Eq. (11.7) is simplified to

$$I(\boldsymbol{x}) = c_{sys} \rho_a \, E_a + c_{sys} E_{ls} [\rho_d \, \boldsymbol{N} \bullet \boldsymbol{L}_s + \rho_s \, p(a_N \boldsymbol{N} \bullet \boldsymbol{V} + a_L \boldsymbol{L}_s \bullet \boldsymbol{V})] . \tag{11.11}$$

Eq. (11.11) is still complicated for analysis. Furthermore, at a Lambertian surface without the ambient illumination, Eq. (11.11) is simply

$$I(\boldsymbol{x}) = c_{sys} E_{ls} \rho_d \, \boldsymbol{N} \bullet \boldsymbol{L}_s . \tag{11.12}$$

In computer vision, a viewer-oriented coordinate system and orthographic projection are often used to further simplify the problem [45]. The viewer-oriented coordinates (X^1, X^2) in the object space are aligned with the image coordinates (x^1, x^2). The third viewer-oriented coordinate X^3 is in the direction of the viewing vector $\boldsymbol{V}$. Eq. (11.12), known as the image irradiance equation in computer vision, has been extensively studied for shape-from-shading [43-44]. For quantitative measurements, Eq. (11.12) can serve as the first-order approximation.

12. Motion Equations of Image Intensity

In this Section, we derive motion equations of image intensity from underlying physical principles. The motion equations of image intensity can be used for recovering the optic flow and other physical properties from a time sequence of images of continuous patterns. The temporal and spatial development of the image intensity depends on the radiation process that is characterized by the physical

parameters $\boldsymbol{p} = (p_1, p_2, \cdots, p_N)^T$ and the geometric parameters $\boldsymbol{q} = (q_1, q_2, \cdots, q_M)^T$, that is,

$$I(\boldsymbol{x}, t) = c_{sys}\, L(\boldsymbol{X}, \boldsymbol{p}, \boldsymbol{q}, t). \tag{12.1}$$

Differentiating Eq. (12.1) with time, we have the motion equation of image intensity

$$\frac{\partial I}{\partial t} + \boldsymbol{u} \bullet \nabla_x I = c_{sys} \left(\frac{\partial L}{\partial t} + \boldsymbol{U} \bullet \nabla_X L + \frac{d\boldsymbol{p}}{dt} \bullet \nabla_p L + \frac{d\boldsymbol{q}}{dt} \bullet \nabla_q L \right) \tag{12.2}$$

where $\boldsymbol{u} = d\boldsymbol{x}/dt$ is the optical flow in the image plane, $\boldsymbol{U} = d\boldsymbol{X}/dt$ is the motion field in the object space, and the gradient operators are defined as

$$\nabla_x = (\partial/\partial x^1, \partial/\partial x^2)^T,$$
$$\nabla_X = (\partial/\partial X^1, \partial/\partial X^2, \partial/\partial X^3)^T,$$
$$\nabla_p = (\partial/\partial p_1, \cdots, \partial/\partial p_N)^T,$$
$$\nabla_q = (\partial/\partial q_1, \cdots, \partial/\partial q_N)^T.$$

The first term in the right-hand side of Eq. (12.2) is the local temporal change of the radiance. The second term is the change induced by motion in a non-homogenous radiance field. The third and fourth terms are related to the changes of the physical and geometric parameters, respectively. Eq. (12.2) is a generic form of the motion equation of image intensity. However, the detailed structure of Eq. (12.2) depends on the specific physical process being studied. To determine the optical flow, Horn and Schunck [46] suggested the well-known brightness constraint equation $\partial I/\partial t + \boldsymbol{u} \bullet \nabla_x I = 0$ in computer vision. In fact, the brightness constraint equation is just an assumption that the image intensity remains invariant along a stream of images. Generally speaking, this assumption, which is not related to any physical process, does not hold exactly. In the following, we give the motion equations of image intensity for three typical cases. Similar results can be obtained for other physical processes. Determining the optic flow in the motion equation of image intensity is a constrained variational problem.

Moving Lambertian Surface

Consider a moving Lambertian surface illuminated by an incident irradiance field $E_{ls}(\boldsymbol{X})$. Since the image intensity is $I(\boldsymbol{x}) = c_{sys} E_{ls} \rho_d\, \boldsymbol{N} \bullet \boldsymbol{L}_s$, the motion equation of image intensity for a Lambertian surface is

$$\frac{\partial I}{\partial t} + \boldsymbol{u} \bullet \nabla_x I = c_{sys}\, \rho_d \left((\boldsymbol{N} \bullet \boldsymbol{L}_s)(\boldsymbol{U} \bullet \nabla_X E_{ls}) + E_{ls} \left(\frac{d\boldsymbol{N}}{dt} \bullet \boldsymbol{L}_s \right) \right). \tag{12.3}$$

The first term in the right-hand side of Eq. (12.3) is the change due to motion in the non-homogenous irradiance field. The term $(d\boldsymbol{N}/dt) \bullet \boldsymbol{L}_s$ represents the rate of change of the unit normal vector $\boldsymbol{N}$ of the surface projected in the illumination directional vector $\boldsymbol{L}_s = (L_{s1}, L_{s2}, L_{s3})^T$. We explore the connection of this term with the fundamental geometric quantities of the surface. The term $(d\boldsymbol{N}/dt) \bullet \boldsymbol{L}_s$ is expanded as

$$\frac{d\boldsymbol{N}}{dt} \bullet \boldsymbol{L}_s = \frac{\partial \boldsymbol{N}}{\partial t} \bullet \boldsymbol{L}_s + \boldsymbol{U} \bullet (\boldsymbol{L}_s \bullet \nabla_X \boldsymbol{N}). \tag{12.4}$$

The surface is described by a parametric equation

$$\boldsymbol{X} = \boldsymbol{X}(\xi^1, \xi^2), \tag{12.5}$$

where ξ^1 and ξ^2 are the parameters of the surface. The term $\boldsymbol{L}_s \bullet \nabla_X \boldsymbol{N}$ can be expressed in ξ^1 and ξ^2

$$\boldsymbol{L}_s \bullet \nabla_X \boldsymbol{N} = L_{s\alpha} \frac{\partial \xi^\beta}{\partial X^\alpha} \frac{\partial \boldsymbol{N}}{\partial \xi^\beta}. \ (\beta = 1,2,\ \alpha = 1,2,3) \tag{12.6}$$

According to the formulae of Weingarten [18]

$$\frac{\partial \boldsymbol{N}}{\partial \xi^\beta} = -g^{\sigma\alpha} b_{\beta\sigma} \frac{\partial \boldsymbol{X}}{\partial \xi^\alpha}, \tag{12.7}$$

we obtain

$$\boldsymbol{U} \bullet (\boldsymbol{L}_s \bullet \nabla_X \boldsymbol{N}) = -l_\beta\, g^{\sigma\alpha} b_{\beta\sigma} \frac{\partial \boldsymbol{X}}{\partial \xi^\alpha} \bullet \boldsymbol{U}, \tag{12.8}$$

where $l_\beta = L_{s\alpha} \partial \xi^\beta / \partial X^\alpha$, $g^{\sigma\alpha}$ are the contravariant metric tensor, and $b_{\beta\sigma}$ are the coefficients of the second fundamental form of the surface.

Emitting Passive Scalar Transport

In a transport process of passive scalar such as fluorescent dye, scattering particles, and temperature in fluids, the radiance is assumed to be proportional to the density or concentration $\psi(\boldsymbol{X}, t)$ of the scalar

$$L(\boldsymbol{X}, t) = c_\psi\, \psi(\boldsymbol{X}, t), \tag{12.9}$$

where c_ψ is a proportional constant. The density of the scalar $\psi(\boldsymbol{X}, t)$ obeys the transport equation

$$\frac{d\psi}{dt} = \frac{\partial \psi}{\partial t} + \boldsymbol{U} \bullet \nabla \psi = D_\psi \nabla_X^2 \psi, \tag{12.10}$$

where D_ψ is the diffusion coefficient of the scalar. Differentiating Eq. (12.1) and using Eqs. (12.9) and (12.10), we have

$$\frac{dI(\boldsymbol{x}, t)}{dt} = c_{sys} c_\psi D_\psi \nabla_X^2 \psi. \tag{12.11}$$

Furthermore, because of $I(\boldsymbol{x}, t) = c_{sys} c_\psi \psi(\boldsymbol{X}, t)$, Eq. (12.11) becomes

$$\frac{dI(\boldsymbol{x}, t)}{dt} = D_\psi \nabla_X^2 I(\boldsymbol{x}, t). \tag{12.12}$$

The Laplace operator ∇_X^2 can be expressed in the image coordinates $\boldsymbol{x}$, i.e.,

$$\nabla_X^2 = h_\gamma \frac{\partial}{\partial x^\gamma} + h_{\gamma\alpha} \frac{\partial^2}{\partial x^\alpha \partial x^\gamma}, \tag{12.13}$$

where h_λ and $h_{\lambda\alpha}$ ($\alpha = 1,2$, $\gamma = 1,2$, $\beta = 1,2,3$) are defined as

$$h_\gamma = \frac{\partial^2 x^\gamma}{\partial X^\beta \partial X^\beta} \text{ and } h_{\gamma\alpha} = \frac{\partial x^\gamma}{\partial X^\beta}\frac{\partial x^\alpha}{\partial X^\beta}. \quad (12.14)$$

For a photogrammetrically calibrated camera, h_γ and $h_{\gamma\alpha}$ are determined by the collinearity equations with the known camera parameters and the image coordinates when a surface constraint $X^3 = F(X^1, X^2)$ is imposed (see Section 4). Hence, the motion equation of image intensity for a passive scalar transport process is

$$\frac{\partial I}{\partial t} + u_\alpha \frac{\partial I}{\partial x^\alpha} = D_\psi \left(h_\gamma \frac{\partial I}{\partial x^\gamma} + h_{\gamma\alpha} \frac{\partial^2 I}{\partial x^\alpha \partial x^\gamma} \right). \quad (12.15)$$

The optical flow field $u^\alpha = dx^\alpha / dt$ can be recovered from Eq. (12.15). In particular, using the orthographic projection $x^\alpha = X^\alpha$, we have

$$h_\gamma = 0 \text{ and } h_{\gamma\alpha} = \delta_{\gamma\alpha}. \quad (12.16)$$

In this case, Eq. (12.15) is reduced to the standard diffusion equation [47]

$$\frac{\partial I}{\partial t} + u_\alpha \frac{\partial I}{\partial x^\alpha} = D_\psi \left(\frac{\partial^2 I}{\partial x^\alpha \partial x^\alpha} \right). \quad (12.17)$$

Transmittant Passive Scalar Transport

Here we derive the motion equation of image intensity for transmittant passive scalar transport in a medium like fluids. When a light ray transmits through a bulk of passive scalar, the intensity of light is attenuated due to absorption and scattering, shown in Fig. 12. The radiance reaching a camera through the scalar medium is given by

$$\frac{dL}{ds} = \boldsymbol{s} \bullet \nabla L = -\beta L, \quad (12.18)$$

where $\boldsymbol{s}$ is the path vector and β is the extinction coefficient. The solution of Eq. (12.18) gives the transmitted radiance

$$L = L_0 \exp\left(-\int_0^s \beta \, ds \right). \quad (12.19)$$

Consider a bulk of the participating passive scalar confined by two virtual boundary surfaces Γ_1 and Γ_2, as shown in Fig. 12. We assume that the camera is far enough away from the bulk of scalar such that the light path is almost parallel to the optical axis, i.e., $\boldsymbol{s} \approx -\boldsymbol{m}_3$. In this case, it is convenient to use the object space coordinates $\overline{\boldsymbol{X}}$ in the frame ($\boldsymbol{m}_1, \boldsymbol{m}_2, \boldsymbol{m}_3$), defined as

$$\begin{aligned} \overline{X}^1 &= \boldsymbol{m}_1 \bullet (\boldsymbol{X} - \boldsymbol{X}_c) \\ \overline{X}^2 &= \boldsymbol{m}_2 \bullet (\boldsymbol{X} - \boldsymbol{X}_c), \\ \overline{X}^3 &= \boldsymbol{m}_3 \bullet (\boldsymbol{X} - \boldsymbol{X}_c) \end{aligned} \quad (12.20)$$

where the unit vectors $\boldsymbol{m}_1$, $\boldsymbol{m}_2$, and $\boldsymbol{m}_3$ are orthogonal, i.e., $m_{\beta\alpha} m_{\gamma\alpha} = \delta_{\gamma\beta}$. Under the above conditions, the transmitted radiance in Eq. (12.19) can be written as

$$L(\overline{\boldsymbol{X}}, t) = L_0 \exp\left(-\int_{\Gamma_1}^{\Gamma_2} \beta(\overline{\boldsymbol{X}}, t) \, d\overline{X}^3 \right), \quad (12.21)$$

where the boundary surfaces are $\overline{X}^3 = \Gamma_1(\overline{X}^1, \overline{X}^2, t)$ and $\overline{X}^3 = \Gamma_2(\overline{X}^1, \overline{X}^2, t)$. The extinction coefficient is proportional to the concentration $\psi(\overline{\boldsymbol{X}}, t)$ of the scalar, i.e.,

$$\beta(\overline{\boldsymbol{X}}, t) = \varepsilon_\psi \, \psi(\overline{\boldsymbol{X}}, t), \quad (12.22)$$

where ε_ψ is an absorption coefficient. The relationship between the image intensity and radiance is

$$I(\boldsymbol{x}, t) = c_{sys} \, L(\overline{\boldsymbol{X}}, t), \quad (12.23)$$

where $\boldsymbol{x} = (x^1, x^2)^T$ is the image coordinates. Combination of Eqs. (12.21), (12.22) and (12.23) yields a basic relation between the image intensity and the concentration of the scalar

$$I(\boldsymbol{x}, t) = c_{sys} L_0 \exp\left(-\varepsilon_\psi \int_{\Gamma_1}^{\Gamma_2} \psi(\overline{\boldsymbol{X}}, t) \, d\overline{X}^3 \right). \quad (12.24)$$

Differentiating Eq. (12.24) with respect to time, we have

$$\frac{dI(\boldsymbol{x}, t)}{dt} = -\varepsilon_\psi \, I(\boldsymbol{x}, t) \left(\int_{\Gamma_1}^{\Gamma_2} \frac{d\psi}{dt} \, d\overline{X}^3 + \psi\big|_{\Gamma_2} \frac{d\Gamma_2}{dt} - \psi\big|_{\Gamma_1} \frac{d\Gamma_1}{dt} \right) \quad (12.25)$$

Since $\psi(\boldsymbol{X}, t)$ obeys the transport equation Eq. (12.10), the first term in the right-hand side is

$$\int_{\Gamma_1}^{\Gamma_2} \frac{d\psi}{dt} \, d\overline{X}^3 = D_\psi \int_{\Gamma_1}^{\Gamma_2} \frac{\partial^2 \psi}{\partial X^\alpha \partial X^\alpha} \, d\overline{X}^3 = D_\psi \int_{\Gamma_1}^{\Gamma_2} \frac{\partial^2 \psi}{\partial \overline{X}^\alpha \partial \overline{X}^\alpha} \, d\overline{X}^3 \quad (\alpha = 1,2,3) \quad (12.26)$$

The second equality in Eq. (12.26) can be easily proven. From Eq. (12.20), we know the differential relation $\partial / \partial X^\alpha = m_{\beta\alpha} \partial / \partial \overline{X}^\beta$ and then

$$\begin{aligned} &\partial^2 / \partial X^\alpha \partial X^\alpha = m_{\beta\alpha} m_{\gamma\alpha} \partial^2 / \partial \overline{X}^\gamma \partial \overline{X}^\beta \\ &= \delta_{\gamma\beta} \, \partial^2 / \partial \overline{X}^\gamma \partial \overline{X}^\beta = \partial^2 / \partial \overline{X}^\beta \partial \overline{X}^\beta \end{aligned}. \quad (12.27)$$

Integration by parts yields

$$\int_{\Gamma_1}^{\Gamma_2} \frac{\partial^2 \psi}{\partial \overline{X}^\alpha \partial \overline{X}^\alpha} \, d\overline{X}^3 = \frac{\partial^2}{\partial \overline{X}^\beta \partial \overline{X}^\beta} \int_{\Gamma_1}^{\Gamma_2} \psi \, d\overline{X}^3 + B.T.,$$

($\beta = 1,2$, $\alpha = 1,2,3$) (12.28)

where the boundary terms $B.T.$ are

$$B.T. = 2\frac{\partial \psi}{\partial \overline{X}^{\beta}}\bigg|_{\Gamma_1} \frac{\partial \Gamma_1}{\partial \overline{X}^{\beta}} - 2\frac{\partial \psi}{\partial \overline{X}^{\beta}}\bigg|_{\Gamma_2} \frac{\partial \Gamma_2}{\partial \overline{X}^{\beta}}$$
$$+ \frac{\partial \psi}{\partial \overline{X}^{3}}\bigg|_{\Gamma_1} \frac{\partial \Gamma_1}{\partial \overline{X}^{\beta}} \frac{\partial \Gamma_1}{\partial \overline{X}^{\beta}} - \frac{\partial \psi}{\partial \overline{X}^{3}}\bigg|_{\Gamma_2} \frac{\partial \Gamma_2}{\partial \overline{X}^{\beta}} \frac{\partial \Gamma_2}{\partial \overline{X}^{\beta}} \quad .$$
$$+ \psi|_{\Gamma_1} \frac{\partial^2 \Gamma_1}{\partial \overline{X}^{\beta} \partial \overline{X}^{\beta}} - \psi|_{\Gamma_2} \frac{\partial^2 \Gamma_2}{\partial \overline{X}^{\beta} \partial \overline{X}^{\beta}} + \frac{\partial \psi}{\partial \overline{X}^{3}}\bigg|_{\Gamma_2} - \frac{\partial \psi}{\partial \overline{X}^{3}}\bigg|_{\Gamma_1}$$

We consider that a bulk of the passive scalar is confined in a finite domain and the distribution of $\psi(\overline{\boldsymbol{X}},t)$ rapidly decrease to zero outside the domain. This represents a typical case in many practical applications. Therefore, when the virtual boundary surfaces Γ_1 and Γ_2 are large enough such that ψ and its derivatives at the surfaces approach to zero, i.e.,

$$\psi|_{\Gamma_1} \to 0\,,\ \psi|_{\Gamma_2} \to 0\,,\ \frac{\partial \psi}{\partial \overline{X}^{\beta}}\bigg|_{\Gamma_1} \to 0\,,\ \frac{\partial \psi}{\partial \overline{X}^{\beta}}\bigg|_{\Gamma_2} \to 0\ . \quad (12.29)$$

Since the boundary terms in Eqs. (12.25) and (12.28) vanish, Eq. (12.25) becomes

$$\frac{dI(\boldsymbol{x},t)}{dt} = -\varepsilon_{\psi} D_{\psi} I(\boldsymbol{x},t) \frac{\partial^2}{\partial \overline{X}^{\beta} \partial \overline{X}^{\beta}} \int_{\Gamma_1}^{\Gamma_2} \psi \, d\overline{X}^{3} \ .$$
$$(\beta = 1,2) \quad (12.30)$$

Now we consider the transformation between the image coordinates $\boldsymbol{x} = (x^1, x^2)^T$ and the object space coordinates $\overline{\boldsymbol{X}} = (\overline{X}^1, \overline{X}^2, \overline{X}^3)^T$. The collinearity equations without the lens distortion are

$$x^{\beta} - x_p^{\beta} = -c\,\overline{X}^{\beta} / \overline{X}^{3} \ . \quad (\beta = 1,2) \quad (12.31)$$

Thus, from Eq. (12.30), the Laplace operator can be written as

$$\frac{\partial^2}{\partial \overline{X}^{\beta} \partial \overline{X}^{\beta}} = \lambda^2 \frac{\partial^2}{\partial x^{\beta} \partial x^{\beta}}\,, \quad (\beta = 1,2) \quad (12.32)$$

where $\lambda = -c / \overline{X}^{3}$ is the scaling factor. Using Eqs. (12.24), (12.30) and (12.32), we obtain the motion equation of image intensity for transmittance images of passive scalar transport

$$\frac{\partial I}{\partial t} + u_{\beta} \frac{\partial I}{\partial x^{\beta}} = D_{\psi} \lambda^2 \left(\frac{\partial^2 I}{\partial x^{\beta} \partial x^{\beta}} - I^{-1} \frac{\partial I}{\partial x^{\beta}} \frac{\partial I}{\partial x^{\beta}} \right).$$
$$(\beta = 1,2) \quad (12.33)$$

Note that a simple version of the motion equation of image intensity for transmittance flow images was given by Wilders et al. [48] based on the orthographic projection and other assumptions.

13. Conclusions

We study a number of theoretical problems in quantitative image-based measurements of geometric, kinematic and dynamic properties of observed objects (specifically deformable bodies). From a unified viewpoint, we discuss different formulations of the perspective projection transformation and their geometrical connection. These equivalent formulations of the perspective projection transformation are selectively used in this paper to study different geometric problems, depending on convenience of the formulation applied to a specific problem. The perspective developable conical surface containing a 3D curve is reconstructed from known image measurements of the curve. The developable conical surfaces can be used to reconstruct a 3D curve and a surface without solving the ambiguous correspondence problem in stereovision. Furthermore, the general methodology is proposed for reconstructing the motion field of a 3D curve from a time sequence of images.

The perspective projection transformation under a surface constraint allows one-to-one mapping between the surface in the object space and the image plane. We explore the connection of the geometric structures and motion fields between the image plane and the surface in the object space. These issues are important in reconstructing the complex motion fields on a surface such as skin friction field on an aerodynamic body and passive scalar motion field illuminated by a laser sheet. Then, we consider the general point correspondence problem in multiple images. Longuet-Higgins relation for the point correspondence problem is generalized by taking the lens distortion effect into account. Generally, establishing the point correspondence requires at least four cameras or images. The concept of the composite image space is introduced. After the relationship between the composite image space and the object space is established under the coplanar condition, the perspective invariants of a 3D curve are constructed. These invariants allow us to directly know the geometric features of the curve such as torsion and curvature from images without calibrating the cameras.

In the radiometric aspects, we discuss the relationship between the image intensity and the radiance received by a camera as well as typical radiation processes such as surface reflection, radiative energy transport through the participating mediums and luminescence. The motion equations of image intensity are derived for moving Lambertian surface, emitting passive scalar transport and transmittant passive scalar transport. These equations provide a rational foundation for recovering the optic flows and motion fields of deformable bodies (e.g. fluids) from a time sequence of images of continuous patterns. Future research will be focused on the development of the effective numerical techniques and algorithms and their implementation in various simulations and experiments.

References

[1] Mikhail, E. M., Bethel, J. S., and McGlone, J. C., Introduction to modern photogrammetry, John Wiley & Sons, Inc., New York, 2001.

[2] Mundy, J. L. and Zisserman, A., Projective geometry for machine vision, in Geometric Invariance in Computer Vision, eds. J. Mundy and A. Zisserman, The MIT Press, Cambridge, 1992.

[3] Faugeras, O., Three-dimensional computer vision, The MIT Press, Cambridge, 1993.

[4] Cipolla, R. and Giblin, P., Visual Motion of Curves and Surfaces, Cambridge University Press, 2000.

[5] Ritter, G. X., Handbook of Computer Vision Algorithms in Image Algebra, CRC Press, Boca Raton, 1996.

[6] McGlone, J. C., Analytic data-reduction schemes in non-topographic photogrammetry, Chapter 4, Non-Topographic Photogrammetry, Second Edition, (H.M. Karara, editor), American Society for Photogrammetry and Remote Sensing, Falls Church, Virginia, 1989, pp. 37-55.

[7] Wong, K. W., Basic mathematics of photogrammetry, Chapter 2, Manual of Photogrammetry, 4th Edition, (C.C. Slama, editor), American Society of Photogrammetry, Falls Church, Virginia, 1980, pp. 37-101.

[8] Wolf, P., Elements of photogrammetry, McGraw-Hill, New York, 1983, pp. 559-601.

[9] Fraser, C. S., Photogrammetric camera component calibration — A review of analytical techniques, Workshop on Calibration and Orientation of Cameras in Computer Vision (TU-1), XVII Congress, International Society of Photogrammetry & Remote Sensing, Washington, DC, 1992.

[10] Fryer, J. G., Camera calibration in non-topographic photogrammetry, Chapter 5, Non-Topographic Photogrammetry, Second Edition, (H.M. Karara, editor), American Society for Photogrammetry and Remote Sensing, Falls Church, Virginia, 1989, pp. 59-69.

[11] Fraser, C. S., Optimization of networks in non-topographic photogrammetry, Chapter 8, Non-Topographic Photogrammetry, Second Edition, (H.M. Karara, editor), American Society for Photogrammetry and Remote Sensing, Falls Church, Virginia, 1989, pp. 95-106.

[12] Abdel-Aziz, Y. I. and Karara, H. M., Direct linear transformation from comparator coordinates into object space coordinates in close-range photogrammetry, Proc. ASP/UI Symp. on Close-Range Photogrammetry, Univ. of Illinois at Urbana-Champaign, Urbana, Illinois, 1971, pp. 1-18.

[13] Tsai, R. Y., A versatile camera calibration technique for high-accuracy 3D machine vision metrology using off-the-shelf TV cameras and lenses, IEEE Journal of Robotics and Automation, Vol. RA-3, No. 4, August, 1987, pp. 323-344.

[14] Liu, T., Cattafesta, L. N., Radeztsky, R. H., and Burner, A. W., Photogrammetry applied to wind-tunnel testing, AIAA J., Vol. 38, No. 6, 2000, pp. 964-971.

[15] Struik, D. J., Lectures on classical differential geometry (Second Edition), Dover, Publications, Inc., New York, 1961.

[16] Batchelor, G. K., An introduction to fluid mechanics, Cambridge University Press, Cambridge, 1988, Chapter 2.

[17] Betchov, R., On the curvature and torsion of an isolated vortex filament, J. Fluid Mech., 22, 1965, pp. 471-479.

[18] Kreyszig, E., Differential geometry, Dover, Publications, Inc., New York, 1991.

[19] Bakker, P. G., Bifurcations in flow patterns, Kluwer Academic Publishers, Boston, 1991.

[20] Dracos, T. and Gruen, A., Videogrammetric methods in velocimetry, *Applied Mechanics Reviews*, Vol. 51, No. 6, 387-413, 1998.

[21] Maas, H. G., Gruen, A., and Papantoniou, D., Particle tracking velocimetry in three-dimensional flows, *Experiments in Fluids*, 15, 133-146, 1993.

[22] Longuet-Higgins, H. C., A computer algorithm for reconstructing a scene from two projections, Nature, Vol. 293, 10, September 1981, pp. 133-135.

[23] Brill, M. H., Barrett, E. B., and Payton, P. M., Projective invariants for curves in two and three dimensions, in Geometric Invariance in Computer Vision, eds. J. Mundy and A. Zisserman, The MIT Press, Cambridge, 1992, Chapter 9.

[24] Springer, C. E., Geometry and analysis of projective spaces, W. H. Freeman and Company, San Francisco, 1964, pp. 18-19.

[25] Holst, G. C., CCD Arrays Cameras and Displays (Second Edition), SPIE Optical Engineering Press, Bellingham, Washington, USA, 1998, Chapter 2.

[26] Haussecker, H., Radiometry of Imaging, in Handbook of Computer Vision and Applications, eds. B. Jahne, H. Haussecker and P. Geisler, Academic Press, San Diego, 1999, Chapters 3 and 5.

[27] McCluney, R., Introduction to Radiometry and Photometry, Artech House, Boston, 1994, Chapter 8.

[28] Nicodemus, F. E., Richmond, J. C., Ginsberg, I. W., and Limperis, T., Geometrical Consideration and Nomenclature for Reflectance, NBS Monograph 160, 1977.

[29] Beckmann, P. and Spizzochino, A., The Scattering of Electromagnetic Waves from Rough Surfaces, Pergamon, New York, 1963.

[30] Icart, I. And Arques, D., Simulation of the Optical Behavior of Rough Identical Multilayers, in Scattering and Surface Roughness III, eds. Z. H. Gu and A. A.

Maradudin, Proceeding of SPIE, Vol. 4100, 2000, pp. 84-95.
[31] Wang, H., Theoretical Analysis and Measurements on Near Specular Scattering, Optics and Laser Engineering, 27, 1997, pp. 285-296.
[32] Torrance, K. E. and Sparrow, E. M., Theory for Off-Specular Reflection from Roughness Surfaces, J. Opt. Soc. Am., Vol. 57, No. 9, 1967, pp. 1105-1114.
[33] Nayar, S. K., Ikeuchi, K. and Kanade, T., Surface Reflection: Physical and Geometrical Perspectives, IEEE Transaction on Pattern Analysis and Machine Intelligence, Vol. 13, No. 7, 1991, pp. 611-634.
[34] Asmail, C., Bidirectional Scattering Distribution Function (BSDF): A Systematized Bibliography, J. of Research of the National Institute of Standards and Technology, Vol. 96, No. 2, March-April, 1991, pp. 512-223.
[35] Gu, Z. H. and Maradudin, A. A., Scattering and Surface Roughness III, Proceeding of SPIE, Vol. 4100, 2000.
[36] Cook, R. L. and Torrance, K. E., A Reflectance Model for Computer Graphics, Computer Graphics, Vol. 15, No. 3, 1981, pp. 307-316.
[37] Phong, B. T., Illumination for Computer Generated Pictures, Commun. ACM, 18, 6, 1975, pp. 311-317.
[38] Modest, M. F., Radiative Heat Transfer, McGraw-Hill, Inc., New York, 1993, Chapters 8, 12, 13, 14, and 15.
[39] Pomraning, G. C., Radiative Hydrodynamics, Pergamon, New York, 1973, pp. 10-49.
[40] Lakowicz, J. R., Principles of Fluorescence Spectroscopy (Second Edition), Kluwer Academic/Plenum Publisher, New York, 1999.
[41] Liu, T., Guille, M. and Sullivan, J., Accuracy of Pressure Sensitive Paint, *AIAA J.*, Vol. 39, No. 1, 2001, pp. 103-112.
[42] Gaigalas, A. K., Li, L., Henderson, O., Vogt, R., Barr, J., Marti, G., Weaver, J., and Schwartz, A., The Development of Fluorescence Intensity Standards, J. of Research of the National Institute of Standards and Technology, Vol. 106, No. 2, March-April, 2001, pp. 381-389.
[43] Horn, B, K. P. and Brooks, M. J., Shape from Shading, The MIT Press, Cambridge, Massachusetts, 1989.
[44] Wolff, L. B., Shafer, S. A., and Healey, G. E., Shape Recovery, Jones and Bartlett Publisher, Boston, 1992.
[45] Horn, B. K. P. and Sjoberg, R. W., Calculating the Reflectance Map, Applied Optics, Vol. 18, No. 11, 1979, pp. 1770-1779.
[46] Horn, B. K. and Schunck, B. G., Determining Optical Flow, Artificial Intelligence, Vol. 17, 1981, pp. 185-204.
[47] Haussecker, H. and Fleet, D. J., Computing optical flow with physical models of brightness variation, IEEE Transaction on Pattern Analysis and Machine Intelligence, Vol. 23, No. 6, June 2001, pp. 661-673.
[48] Wilders, R. P., Amabile, M. J., Lanzillotto, A.-M. and Leu, T.-S., Recovering estimates of fluid flow from image sequence data, Computer Vision and Image Understanding, 80, 2000, pp. 246-266.

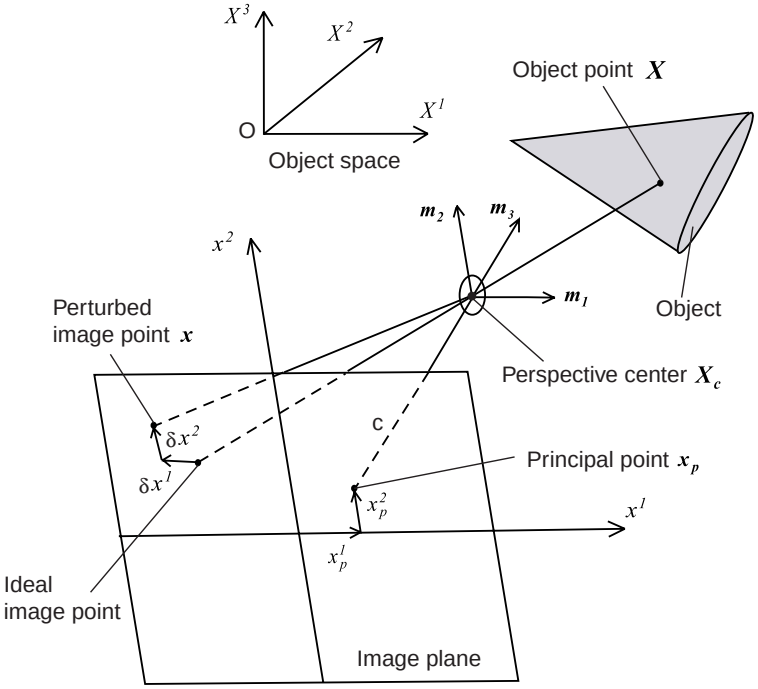

Figure 1. Imaging geometry and coordinate systems.

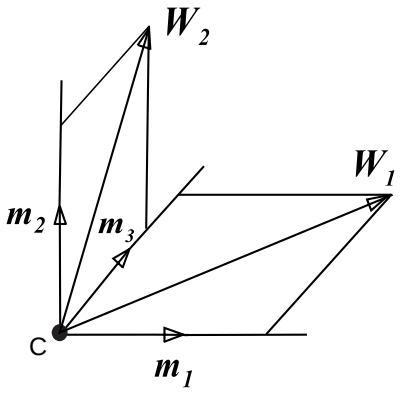

Figure 2. Relationship between the vectors $\boldsymbol{m}_i$ ($i = 1,2,3$) and $\boldsymbol{W}_j$ ($j = 1,2$).

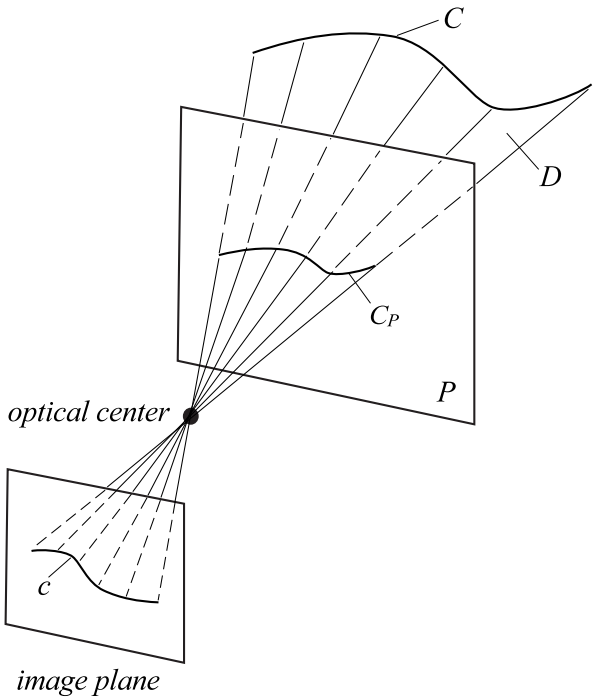

Figure 3. Perspective developable conical surface containing a 3D space curve.

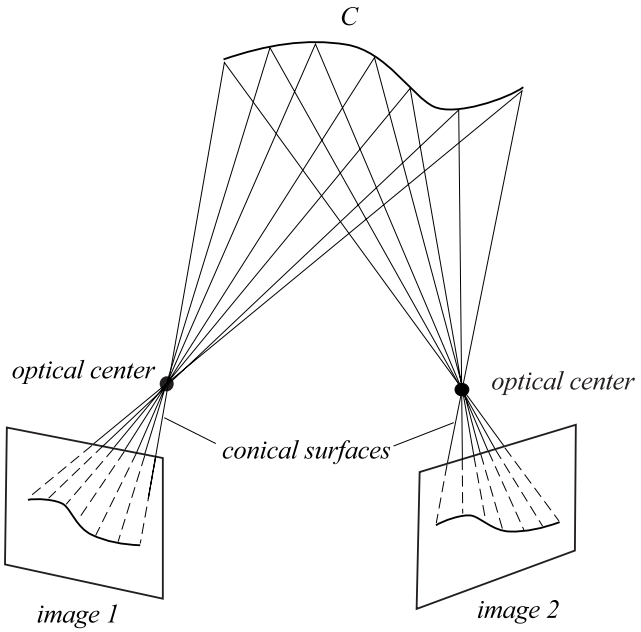

Figure 4. 3D curve as an intersection between two developable conical surfaces.

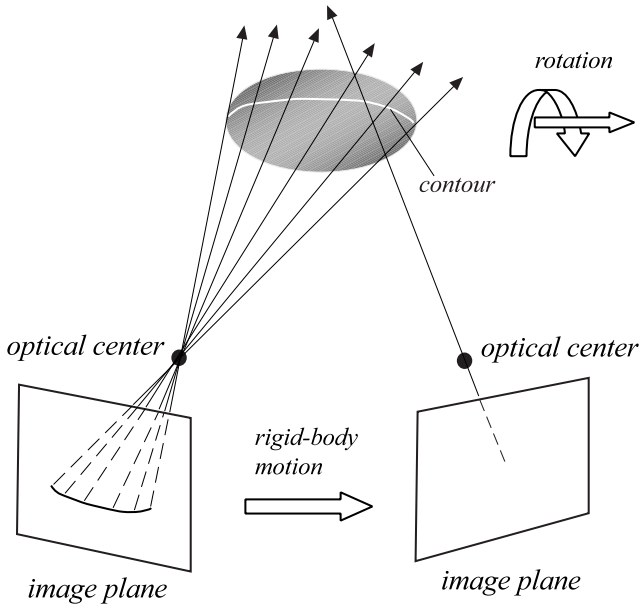

Figure 5. Perspective developable conical surface containing a contour of a 3D surface.

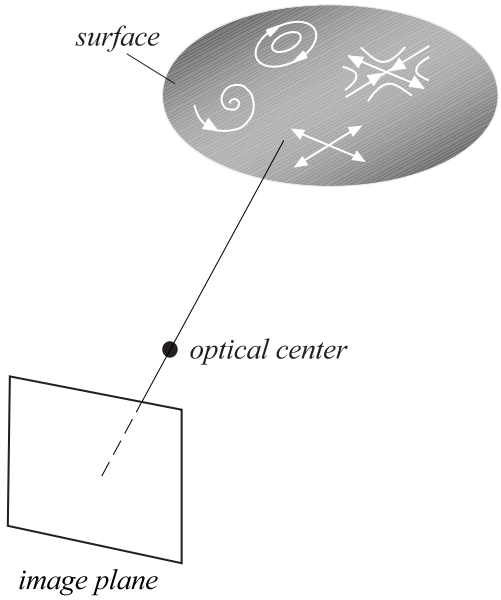

Figure 6. Mapping between 3D surface and image.

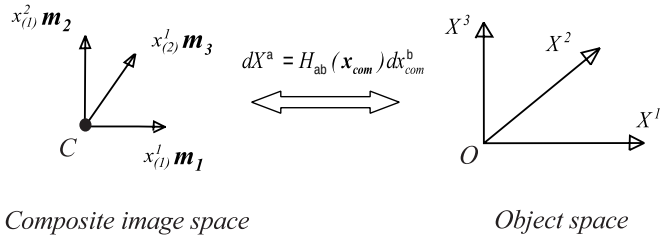

Figure 7. Composite image space and object space.

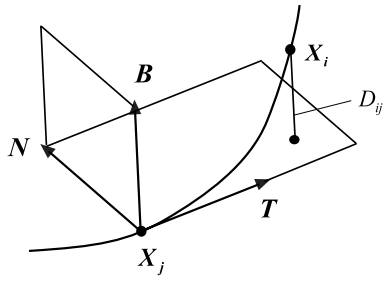

Figure 8. Geometric meaning of the distance D_{ij}.

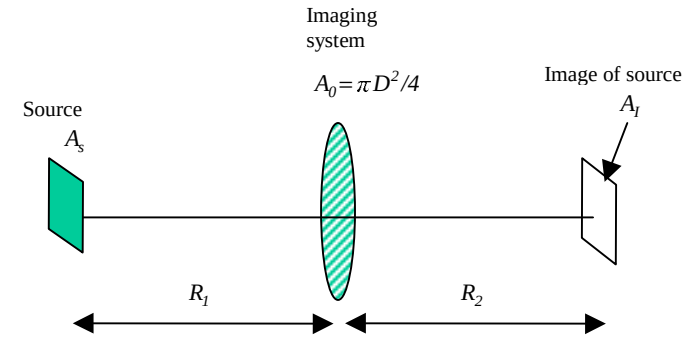

Figure 9. Imaging system.

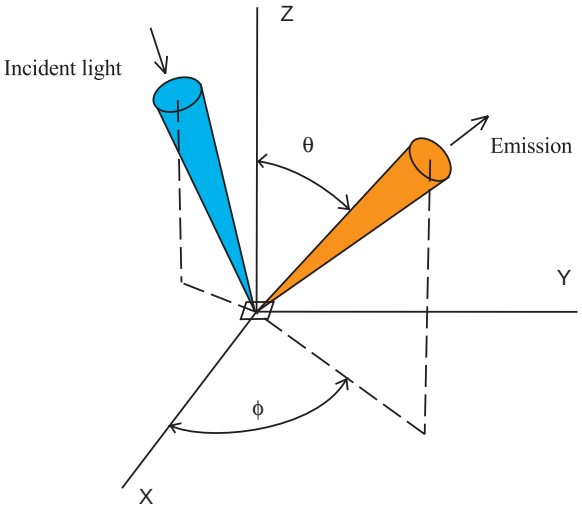

Figure 10. Incident light and reflection in a local coordinate system on a surface.

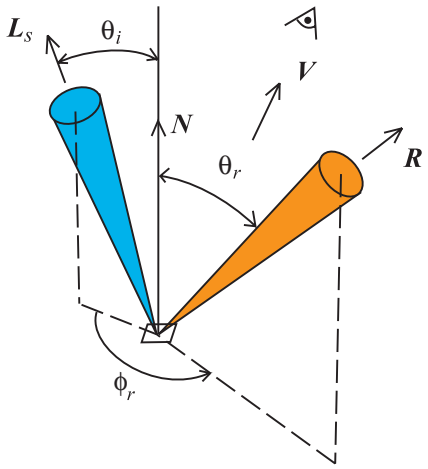

Figure 11. Vectors of incident, reflecting, and viewing directions.

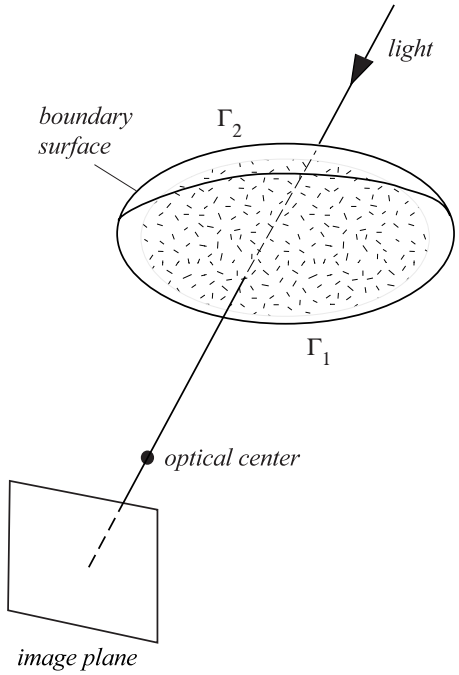

Figure 12. Transmittance of a light ray through passive scalar.